

Temperature-dependent growth contributes to long-term cold sensing

<https://doi.org/10.1038/s41586-020-2485-4>

Received: 13 September 2019

Accepted: 29 May 2020

Published online: 15 July 2020

 Check for updates

Yusheng Zhao^{1,3}, Rea L. Antoniou-Kourouoni^{1,3}, Grant Calder^{1,2}, Caroline Dean¹ & Martin Howard¹

Temperature is a key factor in the growth and development of all organisms^{1,2}. Plants have to interpret temperature fluctuations, over hourly to monthly timescales, to align their growth and development with the seasons. Much is known about how plants respond to acute thermal stresses^{3,4}, but the mechanisms that integrate long-term temperature exposure remain unknown. The slow, winter-long upregulation of VERNALIZATION INSENSITIVE 3 (*VIN3*)^{5–7}, a PHD protein that functions with Polycomb repressive complex 2 to epigenetically silence *FLOWERING LOCUS C* (*FLC*) during vernalization, is central to plants interpreting winter progression^{5,6,8–11}. Here, by a forward genetic screen, we identify two dominant mutations of the transcription factor *NTL8* that constitutively activate *VIN3* expression and alter the slow *VIN3* cold induction profile. In the wild type, the *NTL8* protein accumulates slowly in the cold, and directly upregulates *VIN3* transcription. Through combining computational simulation and experimental validation, we show that a major contributor to this slow accumulation is reduced *NTL8* dilution due to slow growth at low temperatures. Temperature-dependent growth is thus exploited through protein dilution to provide the long-term thermosensory information for *VIN3* upregulation. Indirect mechanisms involving temperature-dependent growth, in addition to direct thermosensing, may be widely relevant in long-term biological sensing of naturally fluctuating temperatures.

Multiple thermosensory pathways have been shown to regulate *VIN3* expression over different timescales^{10,11}, but what accounts for the slow dynamics of *VIN3* as plants experience weeks of cold conditions remains unknown. To investigate this, we identified mutants that showed early cold responses, but could not upregulate *VIN3* over longer periods of cold. A *VIN3-luciferase* translational reporter (Extended Data Fig. 1a) was transformed into a Landsberg *vin3-6* mutant. A single-copy transgenic line, with *VIN3-luciferase* expression similar to endogenous *VIN3* (Extended Data Fig. 1b, c), was selected as the mutagenesis progenitor. The *VIN3-luciferase* reporter substantially rescued the vernalization defect of *vin3-6* (Extended Data Fig. 1d, e).

Two dominant mutants were identified that show high *VIN3* expression in warm conditions (Fig. 1a, b). The mutations, *ntl8-D1* and *ntl8-D2*, prematurely terminated *NTL8* translation and showed morphological defects (with *ntl8-D1* showing more extreme dwarfism and leaf deformation) and high *NTL8* expression (Extended Data Fig. 2a–c), in addition to *VIN3* misexpression. The *ntl8-D* allele dominance suggested that the short *NTL8* proteins without the C-terminal transmembrane domain are constitutively active, as found in studies that link these NAC transmembrane proteins with salt signalling, endoplasmic reticulum stress and trichome development^{12–17}. However, protein truncation is not the only path to ectopic activity, as T-DNA insertions in the *NTL8* promoter also led to *NTL8* overexpression and constitutive *VIN3* expression before cold conditions, but without morphological defects (Extended Data

Fig. 2d–i). *NTL8* binds to *NTL8* and *VIN3* promoter regions *in vitro*¹⁸ and *in vivo* (Fig. 1d, Extended Data Fig. 2j, k). High *VIN3* and *NTL8* expression before cold conditions for *ntl8-D* is thus probably through direct *NTL8* activation.

VIN3 expression was unaffected in the loss-of-function *ntl8-1*. *NTL8* belongs to a 14-member NAC transcription factor subfamily^{14,19–22}. *NTL14* is the closest homologue to *NTL8*, and conditionally induced expression causes ectopic *VIN3* expression¹⁵ (microarray data). Indeed, we identified an *ntl14-D* mutation as constitutively expressing *VIN3* in our *VIN3-luciferase* screen (Extended Data Fig. 3a). We therefore analysed an *ntl8-1 ntl14-1* double loss-of-function mutant and found that *VIN3* cold induction was significantly attenuated (Extended Data Figs. 2e, 3b–d). *ntl8-D* can overcome the vernalization requirement for *FLC* silencing, while *ntl8-1* showed compromised *FLC* silencing and cold acceleration of flowering (Extended Data Fig. 3e–h). These data suggest that the extensive NAC transmembrane family (Extended Data Fig. 3i, j) functions as a redundant network in vernalization and other abiotic responses.

ntl8-D pre-activated *VIN3* expression with limited further increase beyond 1 week of cold exposure (Fig. 1c, Extended Data Fig. 4a). Cold-stress response genes were not consistently affected in *ntl8-D* (Extended Data Fig. 4b–d). Thus, the predominant vernalization role of *NTL8* is in long-term *VIN3* temperature regulation. To assess *NTL8* protein dynamics, we generated transgenics carrying translational

¹John Innes Centre, Norwich Research Park, Norwich, UK. ²Present address: Department of Biology, University of York, York, UK. ³These authors contributed equally: Yusheng Zhao, Rea L. Antoniou-Kourouoni. [✉]e-mail: caroline.dean@jic.ac.uk; martin.howard@jic.ac.uk

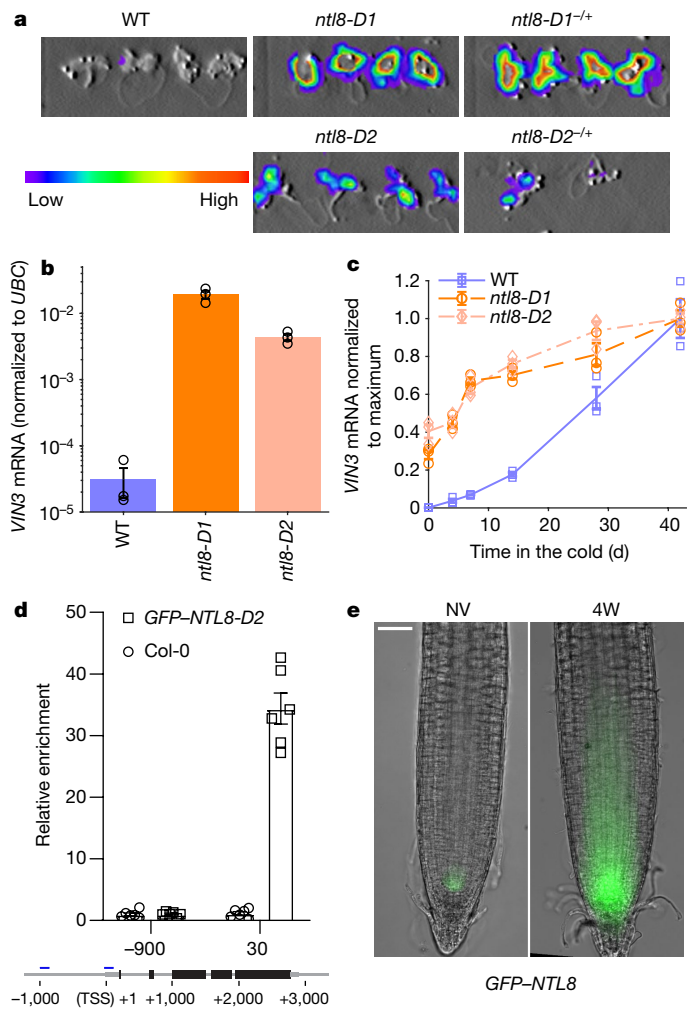


Fig. 1 | Role for NTL8 in long-term cold-induced increase of *V/N3* expression. **a**, Luminescence assay for *ntl8-D1*, *ntl8-D2* before the cold (5 °C) (homozygous and heterozygous (-/+) plants) is shown. Wild type (WT) is the progenitor line carrying transgenic *V/N3-luciferase*. *n*=14 independent repeats with similar results. **b**, Quantitative PCR (qPCR) of *V/N3* transcript levels in warm conditions (20 °C) for WT, *ntl8-D1* and *ntl8-D2*, normalized to *UBC*. Error bars are s.e.m. of three biological replicates (data from the 0-day time point in **c**, not normalized to maximum). **c**, Increase in normalized qPCR *V/N3* transcript levels after different cold durations (5 °C). Levels are normalized to *UBC*, and then to the 42-day time point (maximum *V/N3* level) in each genotype. Error bars are s.e.m. of three biological replicates. **d**, Chromatin immunoprecipitation (ChIP) analysis of NTL8 binding at *V/N3*. Control: Col-0. Error bars are s.e.m. of six replicates. -900, 30: 900 bp upstream, 30 bp downstream of the transcription start site (TSS). **e**, GFP-NTL8 localization in transgenic plant root tips carrying *NTL8prom::GFP-NTL8*. Non-vernalized (NV): 20 °C (left); 4-week cold (4W): 5 °C (right). Scale bar, 50 μm. *n*=5 independent repeats with similar results (including data in Fig. 4d).

GFP fusions to both wild-type and truncated NTL8 proteins. During cold conditions (including fluctuating temperatures), the GFP-NTL8 signal increased in leaves and root meristem regions, coincident with high *V/N3* meristem expression (Fig. 1e, Extended Data Figs. 4e–h, 5a–g). The truncated protein was nuclear-localized in stable transgenics and highly expressed in all cells, probably via NTL8 transcriptional auto-activation (Extended Data Figs. 2c, j, 5b). Wild-type GFP-NTL8 protein was predominantly localized in the plasma membrane and endoplasmic reticulum (around the nucleus) in stable transgenics and *Nicotiana benthamiana* transfection assays¹⁹ (Extended Data Fig. 5b, h). In stable transgenics, there was no change to this subcellular

localization in response to the cold (Extended Data Fig. 5b). Therefore, long-term cold increased the overall NTL8 protein amount, rather than changing the subcellular localization. A fraction of wild-type NTL8 protein must translocate to the nucleus to activate *V/N3*, potentially through cleavage^{12,19} or alternative splicing (Extended Data Fig. 6a–e).

We detected alternatively spliced NTL8 and three GFP-NTL8 protein isoforms (Fig. 2a, Extended Data Fig. 6a, b). Isoform 1 is the full-length NTL8 protein, and shorter isoforms lacked the transmembrane domain. All isoforms increased gradually with weeks of cold, and decreased in post-cold warm, consistent with the long-term *V/N3* cold response. However, isoform 3 showed a faster warm response and could be involved in other temperature pathways that regulate *V/N3* (Fig. 2b, Extended Data Fig. 6b). The gradual increase occurred without a concomitant increase in *NTL8* transcript levels or alternatively spliced transcripts (Fig. 2b, Extended Data Fig. 6c), arguing against transcriptional upregulation or alternative splicing being major factors in gradual NTL8 accumulation in the cold.

To understand slow NTL8-protein accumulation dynamics, we considered the problem theoretically. A single-step cold-induced increase in protein production with fast degradation cannot lead to slow accumulation, as the accumulation timescale is generally dictated by the degradation timescale (Fig. 2c). We therefore explored whether low NTL8 turnover might contribute to its slow accumulation and thus to the gradual increase in *V/N3* expression. Inhibition of translation using cycloheximide revealed that NTL8 isoforms 1 and 2 have half-lives of >2 days in cold and warm conditions, with plants later dying from cycloheximide exposure (Fig. 2d, e, Extended Data Fig. 6f–i). NTL8 therefore always has low turnover, potentially similar to plant proteins with half-lives of months²³.

With slow degradation, the dominant factor determining NTL8 accumulation becomes growth-dependent dilution, as modelled previously for a hormone²⁴. We reasoned that temperature-dependent growth (Extended Data Fig. 7a) could give different patterns of NTL8 accumulation in warm and cold conditions. The total NTL8 amount increases in both conditions (Extended Data Fig. 7b). However, the fast growth in warm conditions before or after cold (Fig. 2a, b, f) could cause rapid NTL8 cellular dilution leading to lower NTL8 concentrations. Slower growth during the cold conditions could enable NTL8 accumulation with higher NTL8 concentrations (Fig. 2a, b).

We developed a mathematical model for the NTL8 concentration in the growing plant (Fig. 3a, Extended Data Fig. 7c–g, Supplementary Methods). At constant temperature, total volume is assumed proportional to time²⁵ (Extended Data Fig. 7a). On the basis of our data, we assigned constant production and very slow degradation of NTL8 protein at all temperatures, or no degradation in the model, and found that this model of indirect temperature sensing through the growth rate could reproduce NTL8 dynamics in warm and cold conditions (Figs. 2, 3b, c). Many aspects of NTL8 biosynthesis are likely to be temperature-regulated, but these would not explain the long-term accumulation. For example, changes to production (such as a global decrease in translation²⁶) influence the final saturated NTL8 concentration, but not the slow accumulation (Fig. 2c, Extended Data Fig. 7c–f). Thus, a key factor for long-term, slow dynamics of NTL8 accumulation in the cold is reduced protein dilution.

A prediction from this model is that inhibiting growth by non-cold treatments would generate similar NTL8 accumulation. Treatment of seedlings with brassinazole, paclobutrazol, hygromycin and a short photoperiod in warm conditions validated this prediction (Fig. 3d–f, Extended Data Figs. 8, 9a–d). NTL8 concentrations increased in treated plants in the warm, with unchanged or even reduced relative RNA levels (Fig. 3e, f). By contrast, NTL8 concentrations were lower following gibberellin treatment in the cold, which accelerates growth¹³ (Extended Data Fig. 9e). The root-tip GFP-NTL8 signal increased in all warm treatments that inhibited growth, except for (almost lethal) hydroxyurea (Extended Data Fig. 8). Furthermore, NTL8 accumulated slowly after

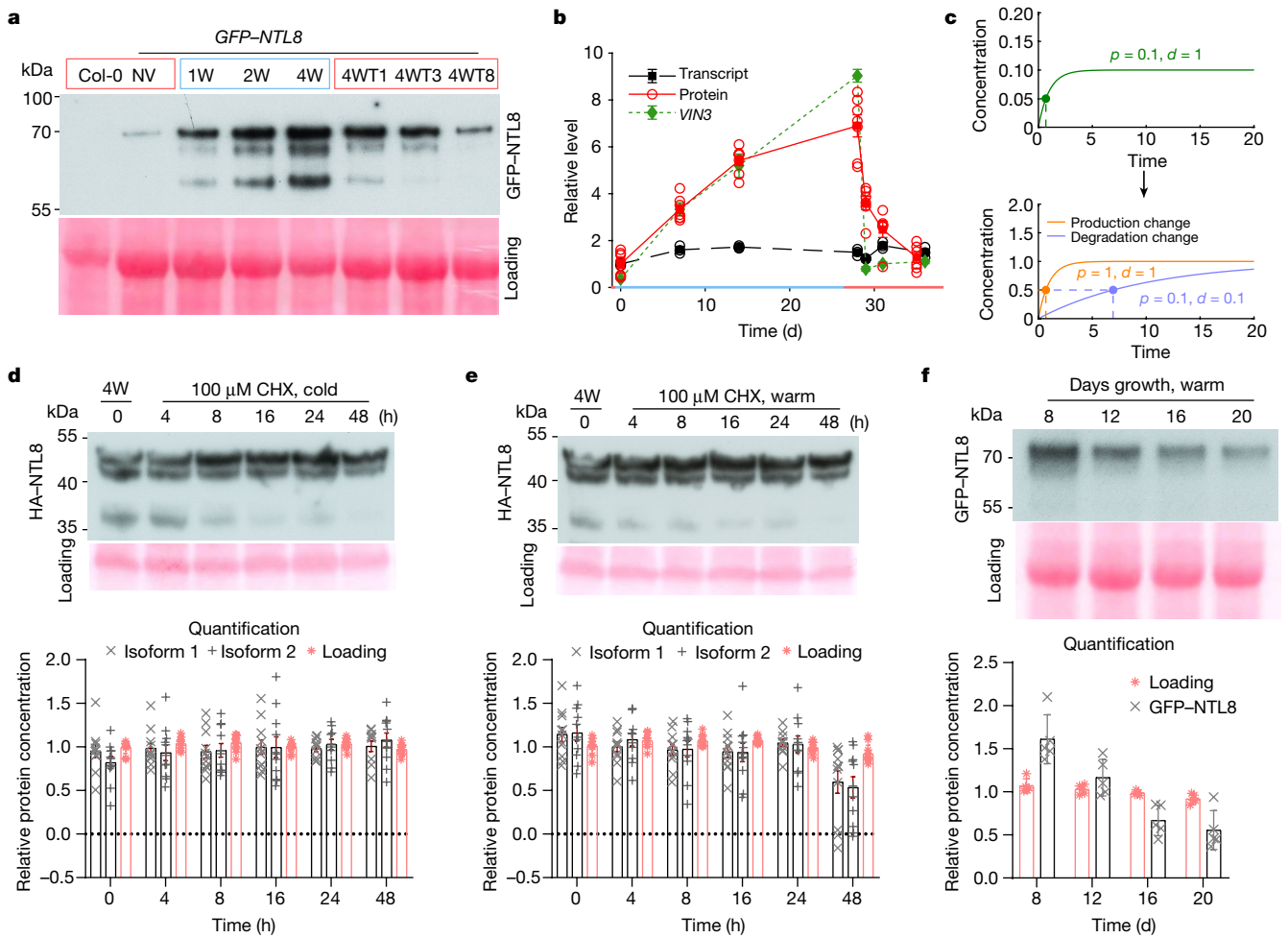


Fig. 2 | NTL8 protein accumulates slowly in the cold with constitutively slow turnover. **a**, Western blot analysis of NTL8 protein in whole plants under different cold durations. Negative control: non-transgenic Col-0. NV: 20 °C. 1W, 2W, 4W: 1, 2, 4 weeks of cold (5 °C). 4WTn: 4 weeks of cold followed by n days warm (20 °C). n=1, 3 and 8. The blue and red rectangles indicate cold and warm conditions, respectively. The experiment was repeated independently seven times with similar results; see Supplementary Fig. 1. **b**, Comparison of *V/N3* transcript dynamics, NTL8 protein and transcript dynamics. NTL8 protein dynamics were measured as the summed intensity of the top two bands (**a**). Transcript levels were determined using samples from the same treatment as **a**. Error bars are s.e.m. of six (*V/N3*), seven (NTL8 protein) and three (NTL8 transcript) biological replicates. NTL8 protein concentration and transcript levels are normalized to NV measurement; *V/N3* transcript levels are normalized to 1 week of cold. The blue and red colours of the x axis indicate cold (5 °C) and warm (20 °C), respectively. **c**, Slow accumulation requires low degradation rates. The simple model (Supplementary Methods) demonstrates

that the time to reach half final concentration ($t_{1/2}$, dashed line) is unchanged by production rate (p) changes but is affected by degradation rate (d) changes. This is a dimensionless model, so it applies regardless of the units of time and concentration. **d, e**, Analysis of NTL8 turnover rate after 4-week cold treatment (5 °C), with subsequent 100 μM cycloheximide (CHX) treatment in cold (**d**) or warm (**e**) (20 °C) conditions for indicated time, with HA-tagged NTL8. Growth was also inhibited by CHX, so measurements reflect protein stability, with little effect from dilution. Quantification: mean ± s.e.m. of 11 biological replicates. The dotted lines intercepting the y axis indicate the background level of the gel and so it is defined as 0. **f**, Western blot analysis of NTL8 protein concentration at different developmental phases in warm conditions (20 °C). Quantification: mean ± s.e.m. of five biological replicates. All western blots were carried out with equal weight of whole seedlings. Ponceau stainings (**a, f**) were run on from separate gels and used as processing controls. Ponceau stainings (**d, e**) from the same gel were used as loading control. For gel source data, see Supplementary Fig. 1.

treatment with the proteasome inhibitor MG132, which also strongly inhibits growth (Extended Data Fig. 9f, g). The fact that varied treatments behaved similarly strongly supports slowed growth as the basis for NTL8 accumulation.

To further explore this concept, we developed a root computational model (Fig. 4a, b, Extended Data Fig. 10a). We postulated that NTL8 is transcribed in a restricted region, as found in recent single-cell transcriptomic analyses²⁷. For such a gene, growth and diffusion can broaden the region in which the protein is detectable²⁸. We applied the same logic, but assumed that diffusion was unlikely to contribute owing to membrane localization of wild-type NTL8 (Extended Data Figs. 4h, 5b) and would not affect the overall NTL8 amount. We found that the

predicted GFP-NTL8 accumulation through reduced growth in the cold matched what was experimentally observed (Fig. 4c, d, Extended Data Fig. 10b, Methods). Furthermore, this root model captured the pattern in warm conditions, with little NTL8 everywhere except the meristems (Fig. 4c, d).

The root model predicted that regions in which NTL8 accumulated during the cold would maintain high levels after warm transfer (Fig. 4e), owing to limited growth in that region combined with long-term NTL8 stability. We verified this key prediction with a high-resolution root time series (Fig. 4f, Extended Data Fig. 10c (i, ii), Supplementary Video 1). Higher growth in the warm led to newly formed tissue having low GFP-NTL8 levels, with high GFP-NTL8 accumulation only at the root tip

Article

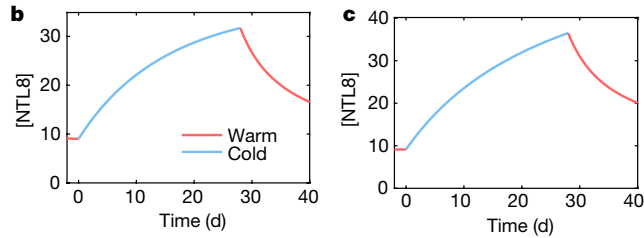
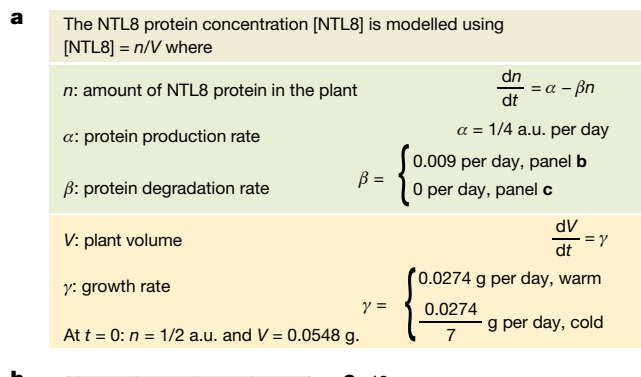
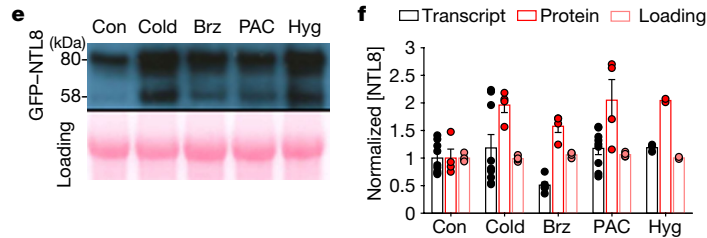
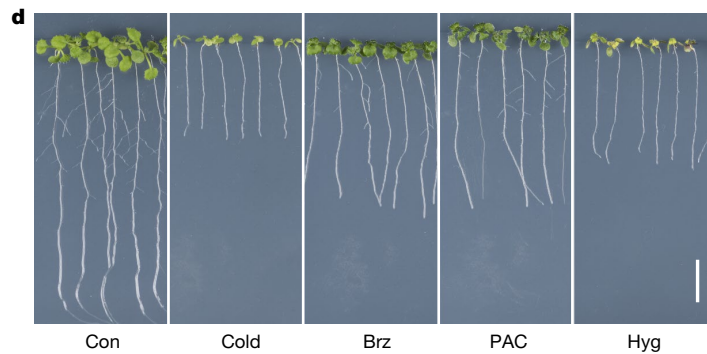


Fig. 3 | Slowing down growth leads to NTL8 accumulation. **a**, Mathematical description of the ordinary differential equation model for NTL8 dynamics. a.u., arbitrary units. **b, c**, Prediction of NTL8 protein concentration dynamics based on a model of **a**: little degradation (**b**) and no degradation (**c**) of the NTL8 protein. **d**, Seedling phenotypes after an 8-day treatment. Brz, brassinazole (20 °C); Con, control (20 °C); Hyg, hygromycin (20 °C); PAC, paclobutrazol (20 °C). Cold: 5 °C. Seedlings were grown for 6 days in warm conditions (20 °C) before transfer to the respective treatment. Images were taken immediately before sampling. Scale bar, 1 cm. **e**, Western blot analysis of NTL8 protein



concentration with treatments in **d** with equal weight of whole seedlings. Ponceau staining was run on separate gels and used as a processing control. The experiment was repeated independently four times with similar results. For gel source data, see Supplementary Fig. 1. **f**, Quantification of relative NTL8 transcript levels and protein concentration in **e**. Error bars are s.e.m. of two (protein in Hyg treatment), four (protein in all other treatments), three (transcript in Hyg treatment), six (transcript in Brz treatment) and nine (transcript in all other treatments) replicates.

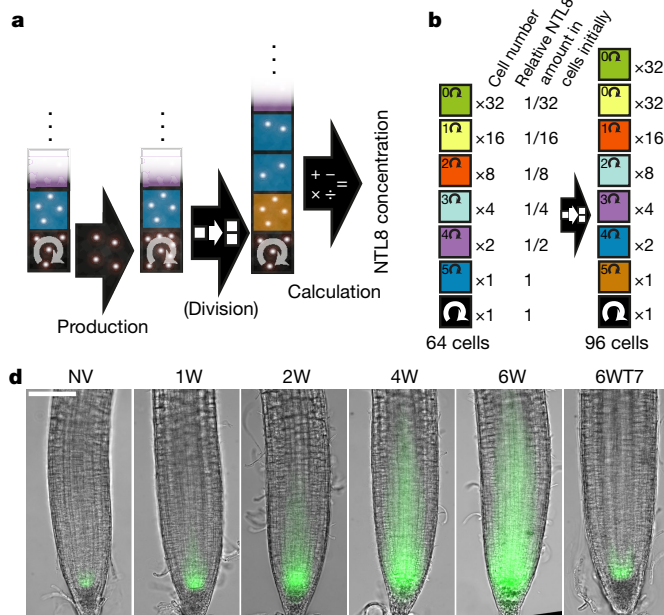
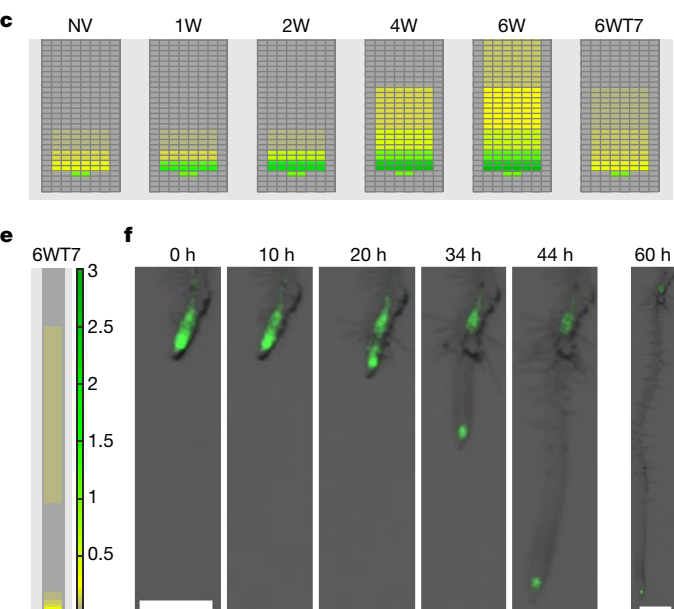


Fig. 4 | Mathematical model predicts observed NTL8 pattern in roots. **a**, Simulation schematic: each day the protein is produced followed, in warm conditions, by division. In cold conditions, division occurs every seventh day. Because division is less frequent, the concentration increases in black cells in cold conditions, spreading through division to other cells. The last step of the simulation each day is calculation/output of the NTL8 protein amount in each cell and the overall root concentration, accounting for the same protein amounts in black and blue cells (and also in the equivalent position in panel **c**: the first two rows above QC, indicated by the two cells in the middle columns). Production occurs in initials only; division following production leads to NTL8 amount split equally between daughters. **b**, Diagram of the model root cell file: each cell from stem cell division is assumed to divide five times. The cell numbers of each type ('Cell number') and the relative NTL8 protein amounts ('Relative NTL8 amount in cells initially') in each cell type are shown



at the simulation start. Inside cells, we indicate the number of divisions to undergo before exiting the 'division zone', with exception of the black cell (initial), which undergoes unlimited divisions. Two generations are shown, indicating 32 cells added at every generation (following a short initial six-generation growth period not included in the simulation). **c**, Model predictions for relative GFP-NTL8 concentrations (using the colour scale bar for concentration in **e**) for the time points shown in **d**. **d**, Images of GFP-NTL8 in roots at the same time points. NV (20 °C); 1W, 2W, 4W, 6W: 1, 2, 4, 6 weeks of cold (5 °C). 6WT7: 6 weeks of cold plus 7 days of warm (20 °C). Scale bar, 100 μm. **e**, Model prediction of the region with NTL8 accumulation during 6 weeks of cold, remaining at high levels for 7 days of post-cold (the colour scale bar for concentration is shown on the right). **f**, Root imaged immediately after 6 weeks of cold (5 °C) (0h) and for 10, 20, 34, 44 and 60 after cold, in warm conditions (20 °C). Scale bar, 500 μm. Five independent repeats for **d** and **f** with similar results.

together with those cells that had arisen during the cold and were no longer growing. Elevated GFP–NTL8 levels in this patch of cells were maintained for 24 days of further growth in the cold (Extended Data Fig. 10c(iii, iv)), underlining that NTL8 protein is stable over weeks.

A combination of experiments and modelling has enabled us to show that reduced protein dilution due to less growth at low temperatures creates a long-term temperature-sensing system. Temperature-dependent growth itself can thus be passively utilized as a long-term thermosensor, naturally averaging temperature fluctuations over long periods. Temperature sensing is distributed broadly through regulatory networks that exploit the temperature dependency of biochemical reactions¹¹. The reduced dilution mechanism is therefore part of this network driving the slow accumulation of NTL8, and thus *VIN3* in the long-term process of vernalization. Such an effect can emerge for any long-lived protein with constant production. It will be important to explore whether other biological processes related to long-term environmental signals use similar mechanisms.

Online content

Any methods, additional references, Nature Research reporting summaries, source data, extended data, supplementary information, acknowledgements, peer review information; details of author contributions and competing interests; and statements of data and code availability are available at <https://doi.org/10.1038/s41586-020-2485-4>.

1. Garrity, P. A., Goodman, M. B., Samuel, A. D. & Sengupta, P. Running hot and cold: behavioral strategies, neural circuits, and the molecular machinery for thermotaxis in *C. elegans* and *Drosophila*. *Genes Dev.* **24**, 2365–2382 (2010).
2. McClung, C. R. & Davis, S. J. Ambient thermometers in plants: from physiological outputs towards mechanisms of thermal sensing. *Curr. Biol.* **20**, R1086–R1092 (2010).
3. Ding, Y., Shi, Y. & Yang, S. Advances and challenges in uncovering cold tolerance regulatory mechanisms in plants. *New Phytol.* **222**, 1690–1704 (2019).
4. Zhang, J., Li, X.-M., Lin, H.-X. & Chong, K. Crop improvement through temperature resilience. *Annu. Rev. Plant Biol.* **70**, 753–780 (2019).
5. De Lucia, F., Crevillen, P., Jones, A. M., Greb, T. & Dean, C. A PHD–Polycomb repressive complex 2 triggers the epigenetic silencing of *FLC* during vernalization. *Proc. Natl Acad. Sci. USA* **105**, 16831–16836 (2008).
6. Sung, S. & Amasino, R. M. Vernalization in *Arabidopsis thaliana* is mediated by the PHD finger protein *VIN3*. *Nature* **427**, 159–164 (2004).
7. Wood, C. C. et al. The *Arabidopsis thaliana* vernalization response requires a Polycomb-like protein complex that also includes VERNALIZATION INSENSITIVE 3. *Proc. Natl Acad. Sci. USA* **103**, 14631–14636 (2006).
8. Michaels, S. D. & Amasino, R. M. *FLOWERING LOCUS C* encodes a novel MADS domain protein that acts as a repressor of flowering. *Plant Cell* **11**, 949–956 (1999).
9. Sheldon, C. C. et al. The *FLF* MADS box gene: a repressor of flowering in *Arabidopsis* regulated by vernalization and methylation. *Plant Cell* **11**, 445–458 (1999).
10. Hepworth, J. et al. Absence of warmth permits epigenetic memory of winter in *Arabidopsis*. *Nat. Commun.* **9**, 639 (2018).
11. Antoniou-Kourounioti, R. L. et al. Temperature sensing is distributed throughout the regulatory network that controls *FLC* epigenetic silencing in vernalization. *Cell Syst.* **7**, 643–655.e9 (2018).
12. Kim, S. G., Kim, S. Y. & Park, C. M. A membrane-associated NAC transcription factor regulates salt-responsive flowering via *FLOWERING LOCUS T* in *Arabidopsis*. *Planta* **226**, 647–654 (2007).
13. Kim, S. G., Lee, A. K., Yoon, H. K. & Park, C. M. A membrane-bound NAC transcription factor NTL8 regulates gibberellic acid-mediated salt signaling in *Arabidopsis* seed germination. *Plant J.* **55**, 77–88 (2008).
14. Tian, H. et al. NTL8 regulates trichome formation in *Arabidopsis* by directly activating R3 MYB genes *TRY* and *TCL1*. *Plant Physiol.* **174**, 2363–2375 (2017).
15. Yang, Z. T. et al. The membrane-associated transcription factor NAC089 controls ER-stress-induced programmed cell death in plants. *PLoS Genet.* **10**, e1004243 (2014).
16. Li, P. et al. Fructose sensitivity is suppressed in *Arabidopsis* by the transcription factor ANAC089 lacking the membrane-bound domain. *Proc. Natl Acad. Sci. USA* **108**, 3436–3441 (2011).
17. Klein, P., Seidel, T., Stocker, B. & Dietz, K. J. The membrane-tethered transcription factor ANAC089 serves as redox-dependent suppressor of stromal ascorbate peroxidase gene expression. *Front. Plant Sci.* **3**, 247 (2012).
18. O’Malley, R. C. et al. Cistrome and epicistrome features shape the regulatory DNA landscape. *Cell* **165**, 1280–1292 (2016).
19. Liang, M. et al. Subcellular distribution of NTL transcription factors in *Arabidopsis thaliana*. *Traffic* **16**, 1062–1074 (2015).
20. Kim, S. Y. et al. Exploring membrane-associated NAC transcription factors in *Arabidopsis*: implications for membrane biology in genome regulation. *Nucleic Acids Res.* **35**, 203–213 (2007).
21. Meng, X. et al. ANAC017 coordinates organellar functions and stress responses by reprogramming retrograde signaling. *Plant Physiol.* **180**, 634–653 (2019).
22. Ng, D. W. K., Abeysinghe, J. K. & Kamali, M. Regulating the regulators: the control of transcription factors in plant defense signaling. *Int. J. Mol. Sci.* **19**, 3737 (2018).
23. Li, L. et al. Protein degradation rate in *Arabidopsis thaliana* leaf growth and development. *Plant Cell* **29**, 207–228 (2017).
24. Band, L. R. et al. Growth-induced hormone dilution can explain the dynamics of plant root cell elongation. *Proc. Natl Acad. Sci. USA* **109**, 7577–7582 (2012).
25. Erickson, R. O. & Michelini, F. J. The plastochron index. *Am. J. Bot.* **44**, 297–305 (1957).
26. Merchante, C., Stepanova, A. N. & Alonso, J. M. Translation regulation in plants: an interesting past, an exciting present and a promising future. *Plant J.* **90**, 628–653 (2017).
27. Zhang, T.-Q., Xu, Z.-G., Shang, G.-D. & Wang, J.-W. A single-cell RNA sequencing profiles the developmental landscape of *Arabidopsis* root. *Mol. Plant* **12**, 648–660 (2019).
28. Mahonen, A. P. et al. PLETHORA gradient formation mechanism separates auxin responses. *Nature* **515**, 125–129 (2014).

Publisher’s note Springer Nature remains neutral with regard to jurisdictional claims in published maps and institutional affiliations.

© The Author(s), under exclusive licence to Springer Nature Limited 2020

Article

Methods

Statistics

No statistical methods were used to predetermine sample size. The experiments were not randomized and investigators were not blinded to allocation during experiments and outcome assessment. Sampling in all cases is performed by collecting material from new plants (not repeated sampling), for replicates and also between time points, with the exception of the time-lapse imaging in Supplementary Video 1.

Plant material and growth conditions

Generally, plant growth conditions were described previously²⁹. For expression analysis and protein extraction, plants were grown on Murashige and Skoog (MS) agar plates without glucose. For microscopy, plants were grown almost vertically on MS plates containing 1% agar. Experiments under the fluctuating temperatures were done as previously described¹⁰.

NTL8 overexpression lines (*ntl8-OE1* (*Salk_866741*) and *ntl8-OE2* (*Salk_587226*)) and the NTL8-knockout line *ntl8-1* (*SM_3_16309*) were obtained from the Nottingham Arabidopsis Stock Centre (NASC). The *NTL14*-knockout line *ntl14-1* (*GT19225*) was obtained from Cold Spring Harbor Laboratory, Cold Spring Harbor, NY, USA (<http://genetrap.cshl.org>). The *35S::HA-NTL8* transgenic line was previously described¹⁴. The *VIN3-luciferase* translational fusions were generated by replacing the stop codon of a *VIN3* genomic fragment (from 6,316 bp upstream of the ATG to 3,095 bp downstream of the stop codon) with a linker and the luciferase coding sequence. The resultant *VIN3-luciferase* reporter was cloned into pSLJ-75516³⁰ and transformed into the *vin3-6* (*vrn7-3*), a Landsberg *erecta* (Ler) mutant²⁹. The transgene copy number was assayed by idnaGENETICS (Norwich Research Park). A transgenic line containing a single-copy transgene and showing a similar expression pattern to the endogenous *VIN3* was selected as the progenitor line for the forward genetic screening. Relevant primers are listed in Supplementary Table 1.

Flowering time analysis

Flowering time analysis was performed as previously described³¹. In brief, plants were grown in containment conditions (16-h light/8-h dark; day temperature: 23–25 °C, and night temperature: 20–22 °C). The total rosette leaf number produced by the main apical meristem before flowering initiation was counted as a measure of flowering time.

Mutagenesis, genetic screening and map-based cloning

Mutagenesis was conducted as previously described³¹. Pooled mutagenesis generation 2 (M2) seeds (from 25 M1 plants) were screened. Approximately 400 seeds from each M2 pool were sown on MS medium and stratified for 3 days in the cold (5 °C). After growth in a growth cabinet for 10 days, the M2 seedlings were sprayed with 1 μM luciferin (E1603, Promega) and assayed for the bioluminescence with a CCD camera (NightOwl). Two mutants were identified (Fig. 1a) and crossed to Col-0 to generate a mapping population. By traditional map-based cloning, both were fine-mapped to a narrow region on chromosome 2 (Extended Data Fig. 10d) and found to carry a mutation in AT2G27300 and so were named *ntl8-D1* and *ntl8-D2*. As *ntl8-D1* was dominant, the WT allele was mapped. SSLP markers for map-based cloning were either from <https://www.arabidopsis.org> or <http://amp.genomics.org.cn>³². A *ntl14-D* mutation was also identified (Extended Data Fig. 3a), and map-based cloning was done in a similar way as for the *ntl8-D* mutations (Extended Data Fig. 10e). The key primers for fine mapping are listed in Supplementary Table 1.

NTL8 constructs and transformation

The *NTL8prom::GFP-NTL8*, *NTL8prom::GFP-NTL8-D1* and *NTL8prom::GFP-NTL8-D2* translational fusions contain a Ler *NTL8* genomic fragment (from 2,278 bp upstream of the ATG to 703 bp

downstream of the stop codon), amplified separately from the progenitor line and the *ntl8-D1* and *ntl8-D2* mutants. The GFP and linker coding sequences were inserted ahead of the ATG of NTL8 by In-Fusion cloning (638909, Takara). The resulting *NTL8prom::GFP-NTL8*, *NTL8prom::GFP-NTL8-D1* and *NTL8prom::GFP-NTL8-D2* were cloned into the binary vector pSLJ-75516³⁰, and transformed into *Agrobacterium* C58. All of the ten randomly selected *NTL8prom::GFP-NTL8* transgenic lines show NTL8 accumulation under cold conditions, and the slow accumulation behaviour is independent of the transgene expression level (Extended Data Fig. 4e–h). The high expression line S4, which carries a single copy of the *NTL8prom::GFP-NTL8* transgene, was used in the paper to facilitate conducting the experiments. Relevant primers are listed in Supplementary Table 1.

Transient assays in *N. benthamiana* were conducted as previously described²⁹. Imaging was done 2 days after infiltration with *Agrobacterium*. For short-term cold treatment, the *N. benthamiana* plants were kept at 5 °C for 2 days after infiltration with *Agrobacterium*. Stable transgenic lines were also generated in Col-0 and plants with a single-copy transgene were selected. Homozygous lines at the T4 generation were used for further experiments.

RNA analysis

Samples were collected at 15:00. Total RNA was prepared as previously described³³. Genomic DNA was removed with TURBO DNA-free (AM1907, Ambion Turbo DNase kit) following the manufacturer's guidelines, before reverse transcription was performed. The reverse transcription was performed with the SuperScript III First-strand Synthesis System (18080-051, Invitrogen) according to the manufacturer's protocol using either gene-specific primers or Oligo(dT)₁₂₋₁₈ (18418-012, Invitrogen). Relevant primers are listed in Supplementary Table 1.

CHX treatment

For the western blot assay in Fig. 2d, e, 4-week vernalized *35S::HA-NTL8* seedlings were soaked in liquid MS medium supplemented with 100 μM CHX (C1988, Sigma-Aldrich) in warm conditions (normal growth cabinet at 20 °C) and cold conditions (vernification cabinet at 5 °C). The seedlings were sampled at the time points of 0 h, 4 h, 8 h, 16 h, 24 h and 48 h. NTL8 proteins were detected as described in 'Protein extraction and western blot assay'.

For the western blot assay in Extended Data Fig. 6f, g, 10-day-old *NTL8prom::GFP-NTL8* seedlings were soaked in liquid MS medium supplemented with 100 μM CHX in warm conditions (normal growth cabinet at 20 °C) and cold conditions (vernification cabinet at 5 °C). Then, approximately 1.0 g seedlings were sampled at the time points of 24 h and 48 h. NTL8 proteins were detected following the procedures in 'Protein extraction and western blot assay'.

For fluorescence imaging, *NTL8prom::GFP-NTL8* seeds were sown on MS medium and grown for 8 days before they were transferred to new MS medium supplemented with 100 μM MG132 (474787, Sigma-Aldrich). After a 24-h or 48-h treatment with MG132 in warm conditions (20 °C), the roots of seedlings were imaged with the standard fluorescence microscope Leica DM6000 and the confocal microscope Leica SP5.

MG132 treatment

NTL8prom::GFP-NTL8 seeds were sown on MS medium and grown for 8 days in warm conditions (20 °C) before they were transferred to new MS medium supplemented with 100 μM MG132 (474787, Sigma-Aldrich). After a 24-h or 48-h treatment with MG132 in warm conditions (20 °C), the roots of seedlings were imaged with the standard fluorescence microscope Leica DM6000. To assess root growth, images were taken with Alpha Innotech Alphaimager. Images before treatment were taken immediately after the transfer, and images after treatment were taken just before the fluorescence imaging.

Microscopy

Confocal imaging was performed using a ×20/0.7 NA multi-immersion lens, with water as the immersion fluid on a Leica TCS SP5 confocal

microscope. For stable transgenic plants, roots were immersed in 2 µg/ml propidium iodide (P4864, Sigma-Aldrich) to label the cell wall. To allow comparison between treatments, the same settings were used for all GFP-NTL8 images, with the exception of Extended Data Fig. 4h, which was imaged with a higher gain value and laser power.

For detecting the fluorescence of GFP-NTL8 in the leaves, confocal imaging was performed using a ×63/1.2 NA water immersion lens on a Leica TCS SP8X confocal microscope. The GFP was excited using 514-nm laser line from a white light laser set to 80 MHz pulse frequency (repeats every 12.5 ns) and fluorescence emission was captured between 525 and 550 nm using a hybrid detector. Time gating was used to remove chloroplast autofluorescence in the green–yellow spectrum³⁴; after an excitation laser pulse, the fluorescence emission of GFP-NTL8 was only detected between 0.47 and 10.80 ns. The chloroplast autofluorescence was used as a marker of the cell, as propidium iodide does not work in the leaf. A z-stack was done to be sure that GFP-NTL8 shows no signal in the leaf under warm conditions. To allow comparison between treatments, the same settings were used for all GFP-NTL8 images.

To compare the fluorescence intensity between roots, imaging was performed using a ×20 lens on a Zeiss Axio Imager fluorescence microscope, which allowed us to collect the total intensity of each root tip. Images taken with the fluorescence microscope Leica DM6000 are specified in the figure legend. To allow comparison between treatments, the same settings were used for all images. Of note, in the comparison of GFP-NTL8 and VIN3-GFP in Extended Data Fig. 5e, VIN3-GFP was imaged with a longer exposure time and higher light intensity.

For imaging the GFP-NTL8 dynamics post-cold (Fig. 4F, Supplementary Video 1), Leica205FA stereomicroscopy was used. Images were taken sequentially around every 10 hours to monitor root growth. To allow the root to grow normally, plants were kept in the growth cabinet in between imaging. To allow comparison between treatments, the same settings were used for all images.

The image processing was conducted with ImageJ: the intensity was linearly adjusted separately for each channel. For visual comparison of the fluorescence intensity between different treatments in the GFP-NTL8 images, the same adjustment was used in ImageJ.

Protein extraction and western blot assay

For *NTL8prom::GFP-NTL8* detection, approximately 1.0 g seedlings were ground to a fine powder in liquid nitrogen. Total protein was extracted by suspending the powder with 2 ml IP buffer (50 mM Tris-Cl pH 8.0, 154 mM NaCl, 10% glycerol, 5 mM MgCl₂, 1% Triton, 0.3% NP-40, 5 mM DTT and protease inhibitor (04693159001, Roche)). After clearing by centrifugation at 16,000g at 4 °C for 20 min, 100 µl total protein was taken as input before enrichment with magnetic GFP-trap beads (GTMA-20, ChromoTek). The input samples were stained with Ponceau buffer and used as a loading control for the initial level for each sample, while enriched GFP-NTL8 protein amounts were detected by western blot. GFP-tagged protein was detected with anti-GFP (11814460001, Roche). Signals were visualized by chemiluminescence (SuperSignal West Femto; 34095, Pierce) using secondary antibodies coupled to horseradish peroxidase (anti-mouse IgG; NXA931V, GE Healthcare). The chemiluminescence signal was captured by exposure to the FUJI Medical X-ray film (4741019289, FUJI). X-ray films for quantification were all scanned with a printer scanner (RICOH). Images of X-ray films shown in Fig. 2 were taken with a high-resolution camera (Canon). Multiple exposures with different times were performed to avoid signal saturation, and a mildly exposed image was always selected for signal quantification with ImageJ. A constant-sized rectangle was drawn in ImageJ to enclose the band and the intensity inside it was measured. For each blot, the measured values were normalized to the average intensity of all the measurements, to remove systematic variability. Ponceau stainings using Ponceau buffer (P7170, Sigma-Aldrich) for all GFP-NTL8 were from separate gels and used as the same processing controls. For *35S::HA-NTL8* detection, total protein was extracted from

200 mg seedlings with 200 µl IP buffer (same procedure as above), and 20-µl aliquot of each sample was taken for western blot detection with anti-HA-peroxidase (12013819001, Roche) or anti-HA-TAG (3724s, Cell Signalling Technology). The signal visualization was as above except with secondary antibodies coupled to horseradish peroxidase (anti-rabbit IgG; NA934V, GE Healthcare) for anti-HA-TAG. Ponceau stainings for all HA-NTL8 from the same gel were reversibly stained with Ponceau buffer. All of the western blot assays were carried out with equal weight of whole seedlings, except Extended Data Fig. 7b (further details are in ‘Assay of the absolute amount of NTL8’).

ChIP

NTL8 protein ChIP experiments were conducted following the ChIP protocol previously described³⁵. For GFP-tagged NTL8, the immunoprecipitation used GFP-trap beads. For HA-tagged NTL8, the immunoprecipitation used anti-HA magnetic beads (88836, Pierce). DNA was purified and analysed as previously described³⁵. Relevant primers are listed in Supplementary Table 1.

3'RACE for detecting alternative splicing

3'RACE was performed with the FirstChoice RLM-RACE Kit (AM1700, Thermal Fisher Scientific) according to the procedures for 3'RACE. In brief, total RNA extracted from WT seedlings, grown for 8 days in standard growth conditions, was used to perform the reverse transcription with the 3'RACE adaptor provided in the kit. Two rounds of PCR were performed with nested primer to provide more materials and better specificity. The second PCR product was then cloned into the PGEM-T vector system1 (A3600, Promega UK). Multiple single clones were sequenced. Relevant primers are listed in Supplementary Table 1. Sequence information of NTL8 isoform 2 and isoform 3 is listed in Supplementary Table 2.

Growth rate assay by measuring fresh weight

For measuring growth rate in warm conditions (20 °C), bulk fresh weight of 50 seedlings was measured at a series of time points (8, 12, 16 and 20 days after moving into the growth cabinet (20 °C)). For measuring growth rate in the cold, seedlings were first grown in the normal growth cabinet for either 7 or 12 days before moving into the vernalization cabinet (5 °C). Then, bulk fresh weight of 50 seedlings was measured at a series of time points in the cold (5 °C) (shown in Extended Data Fig. 7a). Residual water on the seedling surface was carefully removed for accuracy. In addition, a fixed number of seeds (150 seeds per petri dish (140-mm triple vent petri dish; Sterili)) was evenly dispersed on the medium with enough space for growth, to avoid variability caused by density.

Growth inhibition by different treatments

To inhibit the growth rate in warm conditions (20 °C), we used phytohormones and inhibitors including 200 µg/l kanamycin (Kan; 60615, Sigma-Aldrich), aminoethoxyvinylglycine (AVG; 1 µM or 10 µM; A6685, Sigma-Aldrich), 1 µM 2,4-dichlorophenoxyacetic acid (24D; D7299, Sigma-Aldrich), 1 mM abscisic acid (ABA; A1049, Sigma-Aldrich), 10 µM indole-3-acetic acid (IAA; I2886, Sigma-Aldrich), Brz (1 µM or 10 µM; SML1406, Sigma-Aldrich), 20 µg/l Hyg (H9773, Sigma-Aldrich), 1-aminocyclopropane-1-carboxylic acid (ACC; 1 µM, 10 µM or 100 µM; 149101-M, Sigma-Aldrich), hydroxyurea (HU; 10 mM or 20 mM; H8627, Sigma-Aldrich) and PAC (2 µM, 20 µM or 100 µM; 43900, Sigma-Aldrich). For imaging GFP-NTL8 in the root tips, approximately 25 seedlings, grown vertically for 6 days in warm conditions (20 °C), were transferred to new medium supplemented with the above chemicals in the warm (20 °C). To assess root growth, images were taken twice with AlphaImager, the first one immediately after the transfer and the second one 2 days later, just before the fluorescence imaging. Fluorescence imaging was performed with the Zeiss Axio Imager as described above. To detect the protein concentration with western blot, seeds were sown on filter

Article

paper to reduce damage during transfer for the treatment. Around 1.5 g of 6-day-old seedlings was transferred to new medium supplemented with the above chemicals. The seedlings were then grown for another 8 days in warm conditions before sampling. The western blot assay was performed following the procedures in 'Protein extraction and western blot assay'.

Short-day and long-day treatments were applied to avoid the widespread side-effects of chemical treatments. Seeds were evenly dispersed on the medium sufficiently distant from one another. After a 3-day stratification in the cold (5 °C), 6-day-old seedlings were transferred to a growth cabinet (Panasonic MLR-352 series), set to either short-day (8-h day/16-h night, light setting 3) or long-day (16-h day/8-h night, light setting 5) conditions for 2 weeks in the warm (20 °C). Images to assess phenotype were taken immediately before growth measurements. Growth under short-day and long-day conditions was measured by bulk weight of 50 fresh seedlings. The western blot assay was performed following the procedures in 'Protein extraction and western blot assay'. As different light conditions have a strong effect on Rubisco abundance, as shown by Ponceau staining, MPK6 (A7104, Sigma-Aldrich) was used as the loading control.

Growth acceleration in the cold (5 °C) with gibberellin treatment

To accelerate the growth rate in the cold (5 °C), we used gibberellin (GA; G7645, Sigma-Aldrich). For imaging GFP-NTL8 in the root tips, approximately 25 seedlings, grown vertically for 6 days in the warm (20 °C), were transferred to new medium supplemented with the above hormone and placed in the cold (5 °C) for 4 weeks. Fluorescence imaging was performed with the Zeiss Axio Imager and quantified as described above.

Assay of the absolute amount of NTL8

To test the absolute amount of NTL8 in plants between warm and cold temperatures, bulk NTL8 protein was measured by western blot from the same number of seedlings with no treatment (8-day seedlings grown in the warm (20 °C)), 8-day cold treatment (5 °C, following the no treatment pregrowth) or 8-day warm treatment (20 °C, following the no treatment pregrowth). The western blot assay was performed following the procedures in 'Protein extraction and western blot assay'.

Automatic fluorescence intensity quantification

Fluorescence microscopy images (such as in Fig. 1e) were analysed to quantify the fluorescence in the root tip region. A threshold (2,600) was applied to the intensity of the fluorescence of GFP-NTL8 and a mask was created based on this threshold. The second largest connected area was selected (the largest being the no-signal area), and the sum intensity of its fluorescence was quantified. The selection was manually inspected, and a small number of roots were excluded (23 images from a total of 629). This simple algorithm was implemented in Python (<http://www.python.org>) using the czifile (<https://www.lfd.uci.edu/~gohlke/>) and scipy.ndimage (<https://www.scipy.org>) libraries. The code is available in Supplementary Data and at <https://github.com/ReaAntKour/NTL8TemperatureGrowth/>.

NTL8 ordinary differential equation model

Effective degradation (or protein removal) has been reported as the sum of decay and dilution³⁹. This statement is usually applied to proteins in cell populations where all cells divide, giving an exponentially increasing number of cells with time, and where production continues in all daughter cells. However, in multicellular organisms, not all cells continue to divide. In particular, for plants, we have an approximately linear growth in time (Extended Data Fig. 7a). Furthermore, the overall rate of protein production over the whole plant can be constant. Here we modelled the total NTL8 protein amount, the total volume of the cell population approximated by the fresh weight of the plants, and

the overall protein concentration, using the equations described in the Supplementary Methods.

Computational root simulation

We then developed a model for the root to try to capture the spatial pattern observed in our imaging. We made simple assumptions for root structure and growth^{37,38}. We assumed that all cells in the division zone divide once per day, consistent with recent measurements of the times between two divisions³⁹. According to our growth measurements in warm and cold conditions (Extended Data Fig. 7a), we assumed that the division rate slows down to once per week in the cold. In both cases, we simulated divisions that occurred simultaneously for simplicity. All cells are assumed to have the same size and the elongation zone was not simulated. These assumptions substantially simplify our model and, as we are primarily interested in the division zone and our observation timescale is much longer than the cell cycle duration, our conclusions should be largely unaffected by these simplifications.

Four cell files are simulated, one each from the stele, endodermal, cortical and epidermal layers (Extended Data Fig. 10a), represented by a rectangular array of cells, with a variable number of rows. As the root is an axisymmetric structure, we simulate only half a cross-section of the root but also show a mirror image in the figures. The lateral root cap and columella cells are ignored by the model but are also shown in Fig. 4c, together with two quiescent centre cells (the latter with a constant protein amount of 1), as visual reference points. We assume that there is no degradation of the protein, in either cold or warm conditions.

Each cell has an associated NTL8 amount. The step size of the simulation is a day and, every day, a constant amount of NTL8 is made (one-third per day) in each initial cell only (Fig. 4a), excluding the epidermis initial. The total production rate in the simulated half root is therefore one per day, and the average production per cell file is one-quarter per day, matching the production rate in the ordinary differential equation (ODE) model.

Following production, every day in the warm or every seventh day in the cold, synchronous cell division occurs in the division zone (Fig. 4a, b, Extended Data Fig. 10a). We assumed that the division zone is made up of 32 cells in each cell file, including the initial cells. This is an approximation since the cell numbers vary, but it is the equivalent of assuming that a cell that comes from the division of an initial cell divides a further five times (Fig. 4b). At each division, for the bottom 32 rows of cells, each row is turned into two adjacent rows (therefore the growth rate in the warm is $V_d = 32$ per day, and the amount present in the parent cell is split equally between the daughter cells. It is straightforward to calculate the relative amount of protein in a simulated cell with a given distance from the root tip under constant conditions (Fig. 4b). For all rows of cells above 32, there is no change to the cell or to the simulated amount of protein contained within.

Each day, after production and (in case it occurs) division, we calculated the amount of NTL8 in each cell and the overall concentration in the root. The latter is defined as the total amount of protein, divided by the number of cells in the simulated half root (including the epidermis).

Initially, the root has 64 rows of cells. In addition, at $t=0$, the amount of NTL8 in the initial cells and those immediately above (excluding the epidermis cell file, which has no NTL8) is chosen to be equal to 2/21. The two rows of cells above those, each have half the initial amount (1/21), and the four above those each have a quarter (1/42) and so forth. Therefore, at $t=0$, the relative amounts in the 64 cells of a cell file are the same as in Fig. 4b, the total amount in each cell file (excluding the epidermis, which has no NTL8) is equal to two-thirds (two times its production rate) and the overall concentration in the root is 1/128.

For the comparison with the ODE model (Extended Data Fig. 10b), the concentration from the computational simulation model was multiplied by $V_d/V_g = 32/0.0274$ and then directly compared to the output of the ODE model that was run with the same pregrowth and vernalization parameters as the other. Therefore, the root average concentration in

the computational simulation matches the ODE model results, apart from changes due to the discontinuity of cell divisions in the simulation (Extended Data Fig. 10b).

Reporting summary

Further information on research design is available in the Nature Research Reporting Summary linked to this paper.

Data availability

Full-scanned images of western blots are provided with the paper. Raw images that support the findings of this study are available at <https://doi.org/10.6084/m9.figshare.12283970>. Source data are provided with this paper.

Code availability

Code is available in Supplementary Data and at <https://github.com/ReaAntKour/NTL8TemperatureGrowth/>.

29. Greb, T. et al. The PHD finger protein VRN5 functions in the epigenetic silencing of *Arabidopsis FLC*. *Curr. Biol.* **17**, 73–78 (2007).
30. Mylne, J. S. et al. LHP1, the *Arabidopsis* homologue of HETEROCHROMATIN PROTEIN1, is required for epigenetic silencing of *FLC*. *Proc. Natl Acad. Sci. USA* **103**, 5012–5017 (2006).
31. Liu, F., Marquardt, S., Lister, C., Swiezewski, S. & Dean, C. Targeted 3' processing of antisense transcripts triggers *Arabidopsis FLC* chromatin silencing. *Science* **327**, 94–97 (2010).
32. Hou, X. et al. A platform of high-density INDEL/CAPS markers for map-based cloning in *Arabidopsis*. *Plant J.* **63**, 880–888 (2010).
33. Box, M. S., Coustham, V., Dean, C. & Mylne, J. S. Protocol: a simple phenol-based method for 96-well extraction of high quality RNA from *Arabidopsis*. *Plant Methods* **7**, 7 (2011).
34. Kodama, Y. Time gating of chloroplast autofluorescence allows clearer fluorescence imaging in planta. *PLoS ONE* **11**, e0152484 (2016).
35. Yang, H. et al. Distinct phases of Polycomb silencing to hold epigenetic memory of cold in *Arabidopsis*. *Science* **357**, 1142–1145 (2017).
36. Alon, U. *An Introduction to Systems Biology* (Chapman & Hall, 2007).
37. Grandjean, O. et al. In vivo analysis of cell division, cell growth, and differentiation at the shoot apical meristem in *Arabidopsis*. *Plant Cell* **16**, 74–87 (2004).
38. Reddy, G. V., Heisler, M. G., Ehrhardt, D. W. & Meyerowitz, E. M. Real-time lineage analysis reveals oriented cell divisions associated with morphogenesis at the shoot apex of *Arabidopsis thaliana*. *Development* **131**, 4225–4237 (2004).
39. Rahni, R. & Birnbaum, K. D. Week-long imaging of cell divisions in the *Arabidopsis* root meristem. *Plant Methods* **15**, 30 (2019).
40. Bouché, F. *Arabidopsis*—root cell types. *Figshare* <https://doi.org/10.6084/m9.figshare.4688752.v1> (2017).
41. The *Arabidopsis* Information Resource (TAIR). Maps for chromosome 2. TAIR, <https://www.arabidopsis.org/servlets/mapper?value=f12k2&action=search> (accessed 15 May 2020).
42. The *Arabidopsis* Information Resource (TAIR). Maps for chromosome 5. TAIR <https://www.arabidopsis.org/servlets/mapper?value=mwd9&action=search> (accessed 15 May 2020).

Acknowledgements We thank E. Wegel for help with microscopy; S. Chen and R. Xie for genetic screening; J. Fozard for guidance on image analysis and discussion; C. Lökvist and all other members in the Dean and Howard groups for critical discussions; S. Wang for providing the HA::NTL8 line; H. Millar for help on protein stability assessment; and M. Trick for bioinformatic analysis of genome resequencing data (*ntl8-D1*). This work was funded by the European Research Council grant ‘MEXTIM’ and supported by the BBSRC Institute Strategic Programmes GRO (BB/J004588/1) and GEN (BB/P013511/1).

Author contributions Y.Z., R.L.A.-K., C.D. and M.H. conceptualized the study. R.L.A.-K. performed RNA extraction and qPCR for Figs. 1c, 3f and Extended Data Fig. 3g. Y.Z. performed all other experiments. G.C. developed fluorescence imaging protocol and assisted with image acquisition. R.L.A.-K. performed all model development and analysis. Y.Z. performed image processing for western blot quantification. R.L.A.-K. performed image analysis of fluorescence intensity. C.D. and M.H. acquired funding. C.D. conducted project administration. C.D. and M.H. supervised the study. Y.Z., R.L.A.-K., C.D. and M.H. wrote the paper.

Competing interests The authors declare no competing interests.

Additional information

Supplementary information is available for this paper at <https://doi.org/10.1038/s41586-020-2485-4>.

Correspondence and requests for materials should be addressed to C.D. or M.H.

Peer review information *Nature* thanks Chris Hellwell, Ari Pekka Mähönen and the other, anonymous, reviewer(s) for their contribution to the peer review of this work.

Reprints and permissions information is available at <http://www.nature.com/reprints>.

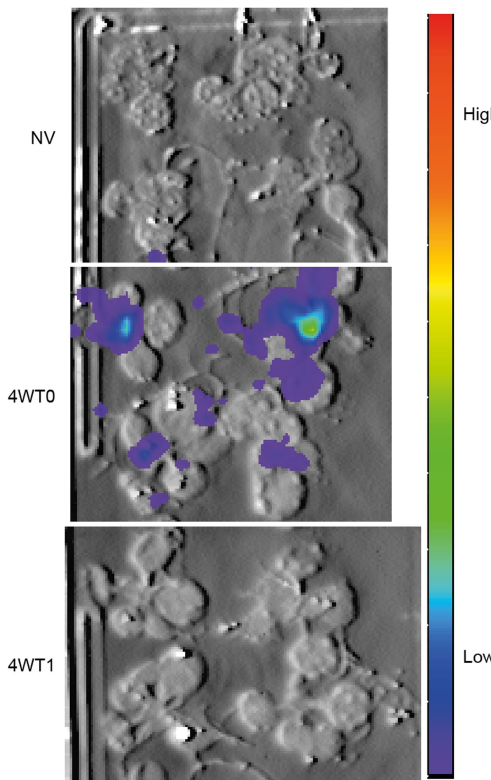
Article

a

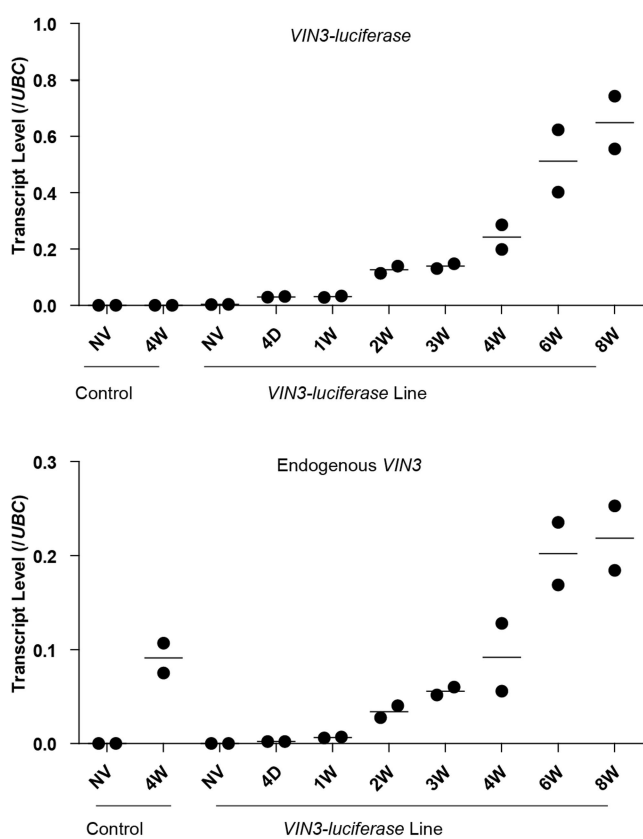
VIN3-luciferase



b



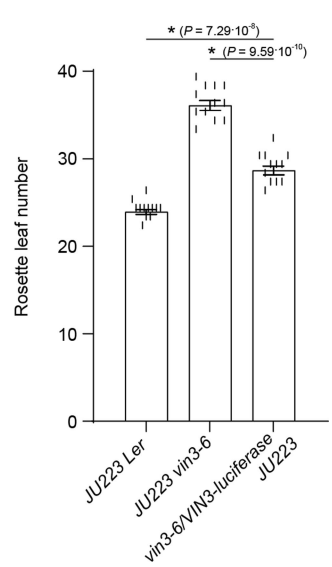
c



d



e



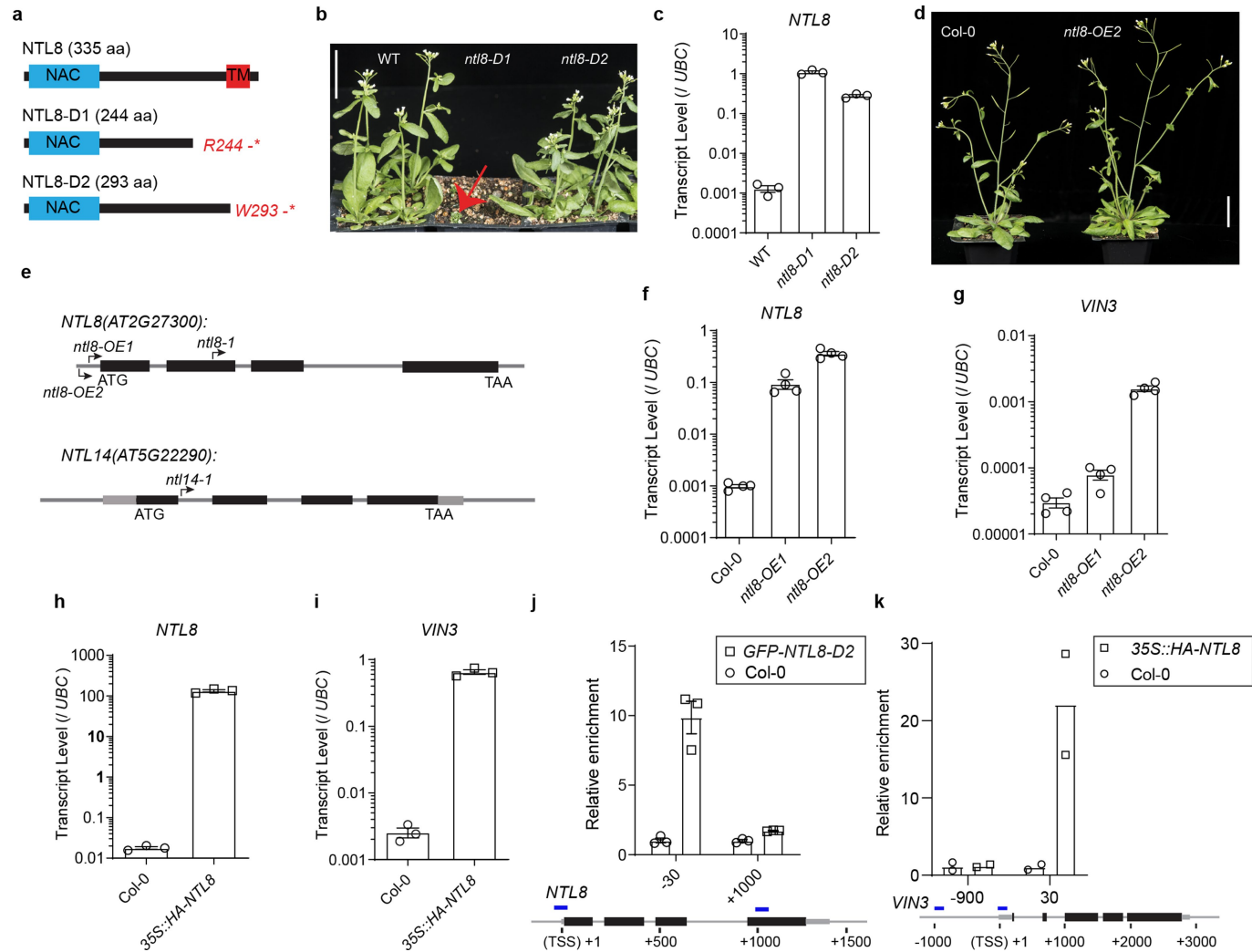
Extended Data Fig. 1 | See next page for caption.

Extended Data Fig. 1 | Characterization of the *VIN3-luciferase* reporter.

a, Schematic for the *VIN3-luciferase* reporter. Luciferase was fused next to the C terminus of *VIN3*. **b**, Luminescence imaging of the transgenic line carrying the *VIN3-luciferase* reporter. NV indicates no cold treatment (20 °C), 4WTO indicates 4 weeks of cold treatment at 5 °C, and 4WT1 indicates 4 weeks of cold plus 1 day of warm treatment at 20 °C. Four independent repeats with similar results were performed. **c**, Analysis of endogenous *VIN3* and transgenic *VIN3-luciferase* transcripts in the reporter line under different lengths of cold treatment (5 °C). Control indicates the non-transgene *vin3-6* control. 4D

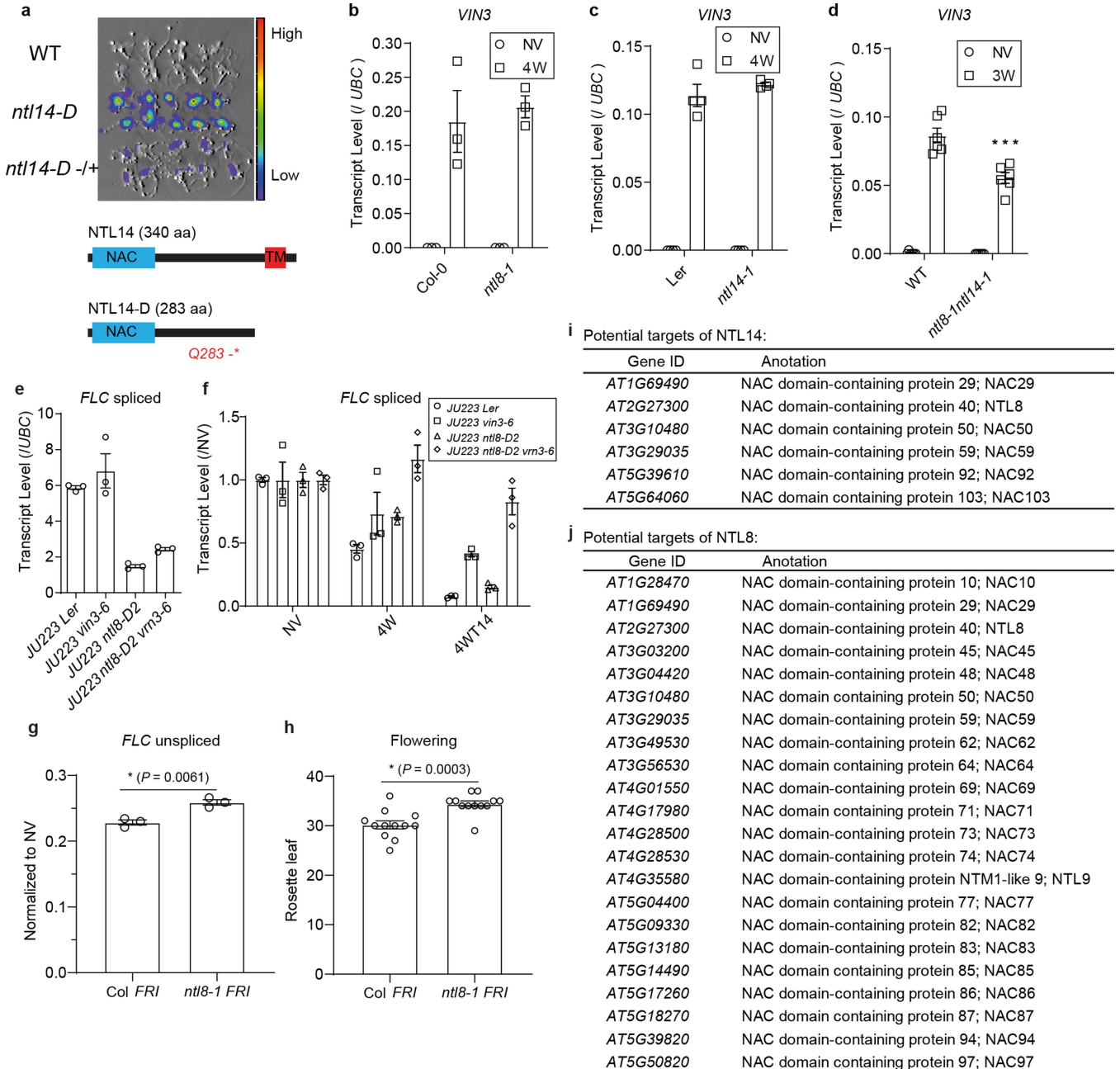
indicates 4 days of cold treatment. *nW* indicates *n* weeks cold treatment, in which *n* is 1, 2, 3, 4, 6 or 8. Two biological replicates (dots) and their means (lines) are shown. **d, e**, Flowering phenotype of the reporter line after 4 weeks of vernalization (5 °C). *JU223*, a *FR1* transgene, was introduced into the reporter line by crossing. Error bars are s.e.m. of 12 individuals. Analysis of variance (ANOVA) with Tukey honest significant difference (HSD) post hoc test for multiple comparisons was performed, and *P* values for individual comparisons of interest are shown. Scale bar, 2.5 cm.

Article



Extended Data Fig. 2 | Characterization of ntl8-D1, ntl8-D2 and NTL8 overexpression lines. **a**, Schematic of the predicted proteins with the identified mutations in *ntl8-D1* and *ntl8-D2* mutants. The light blue box indicates the NAC (NAM/ATAF/CUC) domain, and the red box indicates the transmembrane domain (TM). R indicates arginine, W indicates tryptophan, and the asterisk indicates the stop codon. aa, amino acid. **b**, Developmental phenotypes of *ntl8-D1* (indicated by the red arrow) and *ntl8-D2* mutants. Scale bar, 2.5 cm. Three independent repeats with similar results were performed. **c**, *NTL8* transcript quantification in WT and *ntl8-D1* and *ntl8-D2* mutants in the warm (20 °C). Errors are s.e.m. of three biological replicates. **d**, No morphological phenotype is observed in the *ntl8-OE2* mutant. Scale bar, 2.5 cm. Five independent repeats with similar results were performed. **e**, Schematic of the T-DNA mutant *SM_3_16309(ntl8-1)*, *Salk_866741(ntl8-OE1)*,

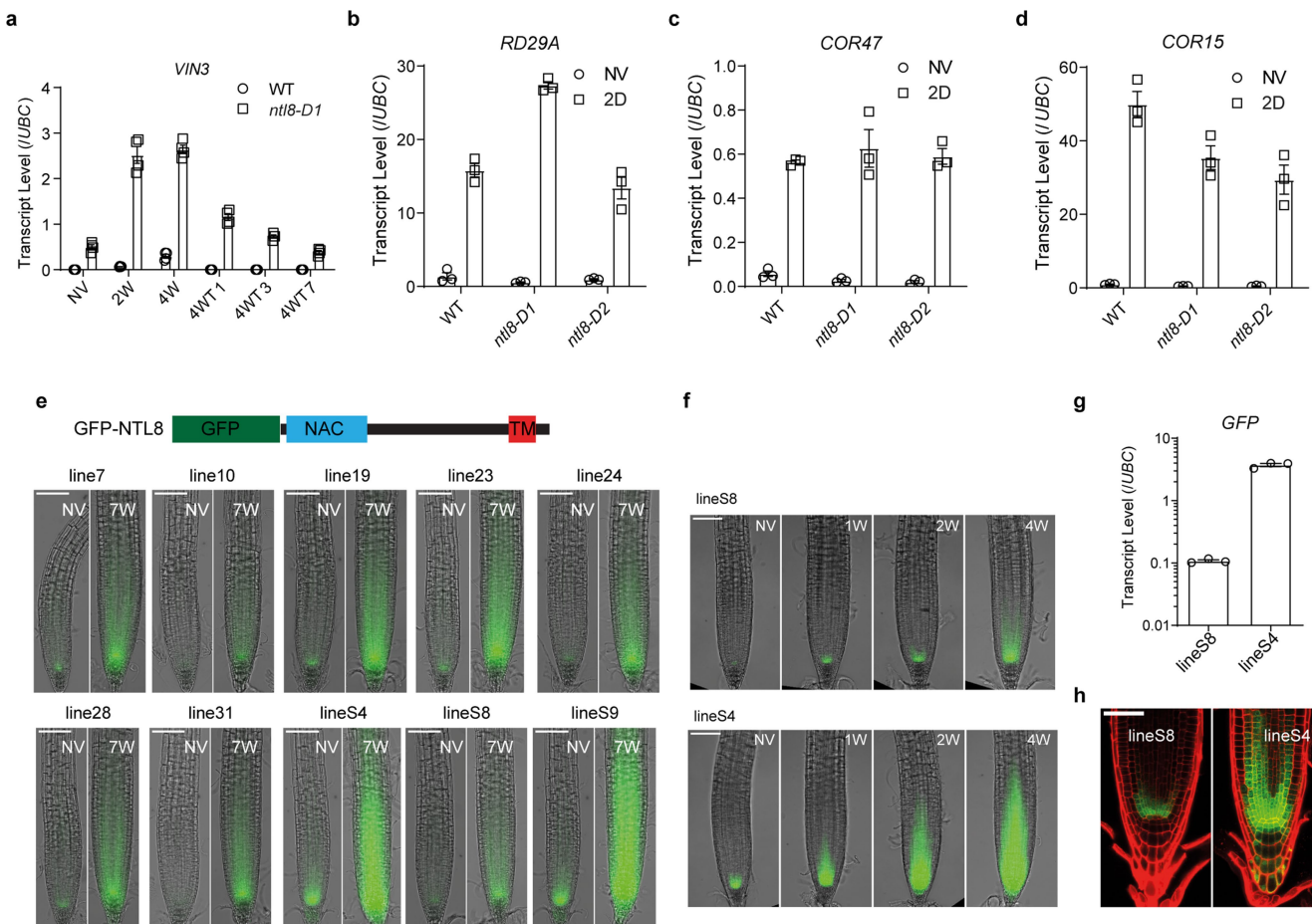
Salk_587226(ntl8-OE2) and *GT19225(ntl14-1)*. **f**, Analysis of the *NTL8* transcript by qPCR in *ntl8-OE1* and *ntl8-OE2* in the warm (20 °C). **g**, Analysis of the *VIN3* transcript by qPCR in *ntl8-OE1* and *ntl8-OE2* in the warm (20 °C). For **f**, **g**, error bars are s.e.m. of four biological replicates. **h**, Analysis of the *NTL8* transcript in the *35S::HA-NTL8* transgenic line. **i**, Analysis of the *VIN3* transcript in the *35S::HA-NTL8* transgenic line in the warm (20 °C). For **h**, **i**, error bars are s.e.m. of three biological replicates. **j**, Analysis of *NTL8* binding at the *NTL8* locus by ChIP. Col-0 was used as a background control. Error bars are s.e.m. of three replicates. Primer positions are shown in the *NTL8* schematic below (-30: 30 bp upstream, +1,000: 1,000 bp downstream of the TSS). **k**, Analysis of *NTL8* binding at the *VIN3* locus by ChIP. Primer positions are shown in the *VIN3* schematic below (-900: 900 bp upstream, 30: 30 bp downstream of the TSS, as in Fig. 1d). Two biological replicates are shown.



Extended Data Fig. 3 | Role of NTL8 in vernalization and redundancy.

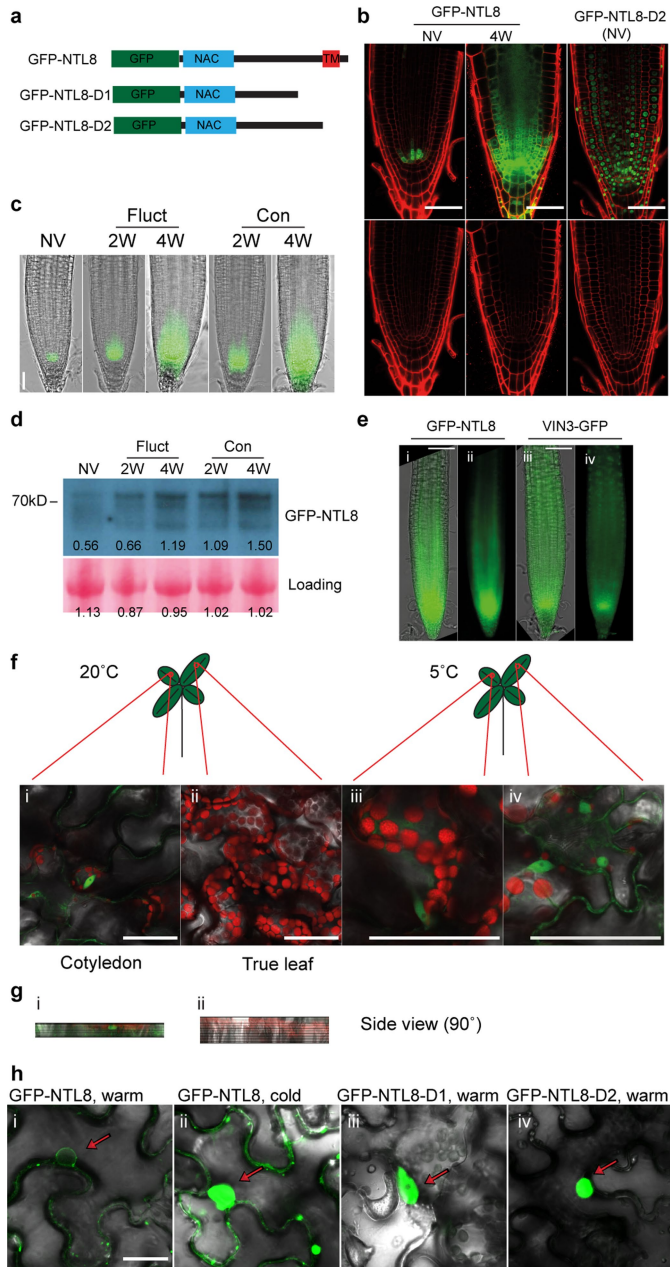
a, Forward genetics identified *ntl14-D*. A schematic of NTL14 is shown below. The light blue box indicates the NAC domain, and the red box indicates TM. Q indicates glutamine, and the asterisk indicates the stop codon. Seven independent repeats with similar results were performed. **b**, Analysis of *VIN3* transcript level by qPCR in the *ntl8-1* mutant and the Col-0 control, at NV (20 °C) and 4 weeks of cold treatment (4W) at 5 °C. Error bars show s.e.m. of three biological replicates. **c**, As for b, but in *ntl14-1* and the Ler control. Error bars show s.e.m. of four biological replicates. **d**, *VIN3* transcript in *ntl8-1ntl14-1* and WT control, at NV (20 °C) and 3 weeks of cold treatment (5 °C). WT, WT plants in the F2 population of the cross between *ntl8-1* and *ntl14-1*. For comparison between WT and the *ntl8-1ntl14-1* double mutant, we performed a two-tailed t-test: $t = 4.634$, d.f. = 10, $P = 0.0009$. Error bars show s.e.m. of six biological replicates. **e**, **f**, Analysis of *FLC* transcripts in Ler JU223, *vin3-6* JU223, *ntl8-D2*

and *ntl8-D2 vin3-6* JU223 mutants under NV (e), 4WT0 (f) and 4WT14 (f) conditions. NV indicates the warm (20 °C) before cold treatment, 4W indicates 4 weeks of cold treatment at 5 °C, and 4WT14 indicates 4 weeks of cold plus 14 days of warm treatment at 20 °C. In f, data are normalized to the corresponding NV treatment. Error bars are s.e.m. of three biological replicates. **g**, Unspliced *FLC* levels after 4 weeks of vernalization in Col FRI and *ntl8-1 FRI*, normalized to the NV levels in the same genotype. Error bars are s.e.m. of three biological replicates. Unpaired t-test, two-tailed: $t = 5.303$, d.f. = 4, $P = 0.0061$. **h**, Flowering time, counted by the number of rosette leaves at flowering, for plants vernalized for 4 weeks. Error bars are s.e.m. of 12 individuals. Unpaired t-test, two-tailed: $t = 4.241$, d.f. = 22, $P = 0.00031$. **i**, Potential cross-regulation targets of NTL14 based on microarray data¹⁷. **j**, Potential cross-regulation targets of NTL8 based on in vitro data²⁰. RNA was isolated from whole seedlings, and values are all normalized to UBC.



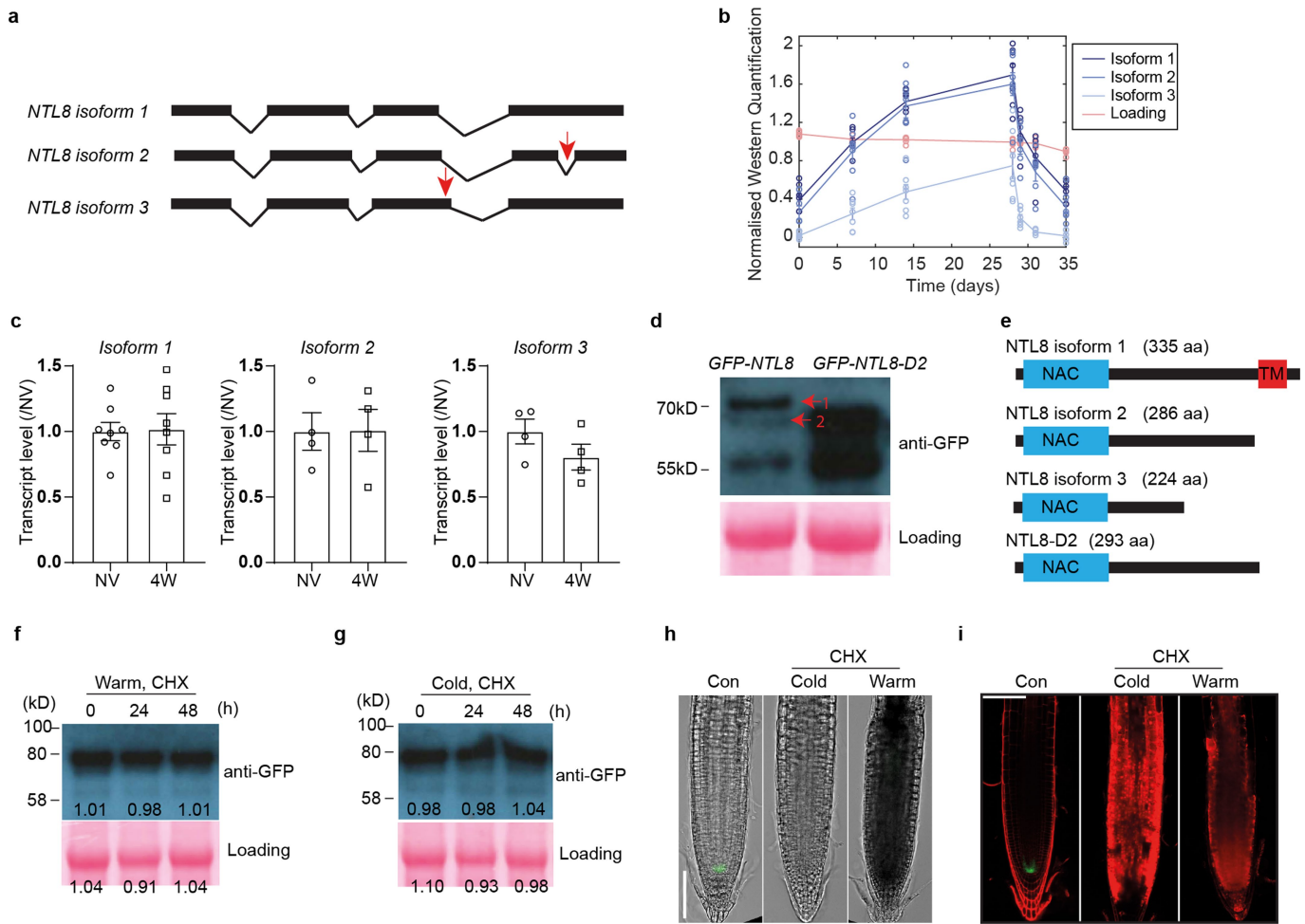
Extended Data Fig. 4 | Analysis of *VIN3* and short-term cold stress-inducible genes in *ntl8-D* mutants, and characterization of independent *NTL8prom::GFP-NTL8* transgenic lines. **a**, Analysis of *VIN3* transcript level under different lengths of cold treatment by qPCR. 4WTn indicates 4 weeks of cold at 5 °C plus n days of warm at 20 °C, in which n is 1, 3 or 7. NV: 20 °C. Data are normalized to *UBC*. Error bars are s.e.m. of four biological replicates. **b-d**, *RD29A* (**b**), *COR47* (**c**) and *COR15* (**d**) transcript quantification in WT and *ntl8-D* mutants. NV indicates no cold treatment (20 °C), and 2D indicates 2-day cold treatment at 5 °C. Error bars are s.e.m. of three biological replicates. **e**, All ten randomly selected *NTL8prom::GFP-NTL8* transgenic lines show NTL8 accumulation in the cold. 7W refers to 7 weeks of cold at 5 °C. Scale bars, 100

f, Two representative lines showing the slow accumulation behaviour of NTL8 in the cold. 1W, 2W and 4W refer to 1, 2 and 4 weeks of cold, respectively, at 5 °C. Scale bars, 100 µm. Two independent repeats with similar results were performed. **g**, The transcript level of the *NTL8prom::GFP-NTL8* transgene in the two representative lines S4 and line S8. Values are normalized to *UBC*. Error bars are s.e.m. of three biological replicates. RNA was isolated from whole seedlings. **h**, Detection of low GFP-NTL8 levels in NV plants after long exposure. Propidium iodide staining was used to mark the root structure. Scale bar, 50 µm. Five roots were assayed with similar results.



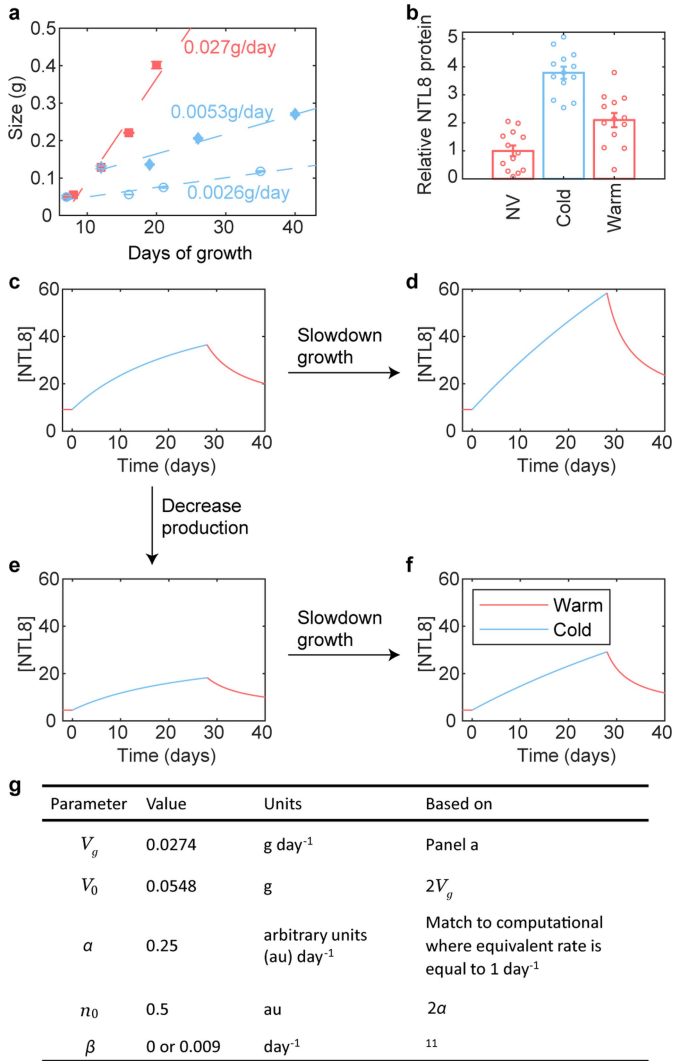
Extended Data Fig. 5 | Subcellular and tissue localization of NTL8 protein.

a, Schematics of the GFP-NTL8, GFP-NTL8-D1 and GFP-NTL8-D2 proteins. A GFP linker was fused at the N terminus of NTL8, NTL8-D1 and NTL8-D2. **b**, Localization of GFP-NTL8 and GFP-NTL8-D2 in the root in stable transgenic plants (top) and only the propidium iodide staining channel for the same roots (bottom), indicating that they are the same optical section. Eight-day-old roots were imaged with Leica SP5 confocal microscopy. NV: 20 °C, and 4W indicates 4 weeks of treatment in the vernalization room at 5 °C. Propidium iodide staining was used to mark the root structure. Scale bars, 50 µm. Four independent repeats with similar results were performed. **c, d**, NTL8 accumulation after exposure to fluctuating temperatures. In **c**, imaging of the GFP-NTL8 fluorescence signal in the root tip with a Leica DM6000 microscope, under exposure to different lengths of fluctuating temperatures (Fluct; with an average temperature of 14 °C) and constant temperature of 14 °C (Con) is shown. Scale bar, 50 µm. Independent roots ($n = 6$ for NV, 12 for Con-2W, 13 for Fluct-2W, 4 for Con-4W and 5 for Fluct-4W) were assayed with similar results. In **d**, analysis of the GFP-NTL8 protein using western blot after the same conditions as in **c** is shown. One replicate is represented. Ponceau staining of the input on a separate gel was used for the loading control. Quantification of band intensity is shown on each gel. For gel source data, see Supplementary Fig. 1. **e**, Domains of NTL8 (i and ii) and VIN3 (iii and iv) in the root tip after 7 weeks of cold. i and iii show the merged image of bright-field and fluorescence channels, and ii and iv show the fluorescence channel only. Scale bars, 100 µm. Independent roots ($n = 5$ for GFP-NTL8 and 13 for VIN3-GFP) were assayed with similar results. **f**, Detection of the GFP-NTL8 fluorescence signal in the shoot in warm conditions (20 °C) or after 6 weeks of cold (5 °C). Green indicates the signal of GFP-NTL8, red indicates the signal from chlorophyll autofluorescence, and grey indicates the bright-field. Scale bars, 50 µm. **g**, i and ii are the side view of the 3D projection of **f**(i) and **f**(ii), respectively. Three independent repeats with similar results were performed. **h**, Subcellular localization of GFP-NTL8, GFP-NTL8-D1 and GFP-NTL8-D2 with a transient assay in *N. benthamiana*. GFP-NTL8 (i), GFP-NTL8-D1 (iii) and GFP-NTL8-D2 (iv) were kept in warm (20 °C) conditions for 2 days before imaging; GFP-NTL8 (ii) was kept in the cold (5 °C) for 2 days before imaging. The arrows point to nuclei. Scale bar, 25 µm. Two independent repeats with similar results were performed.

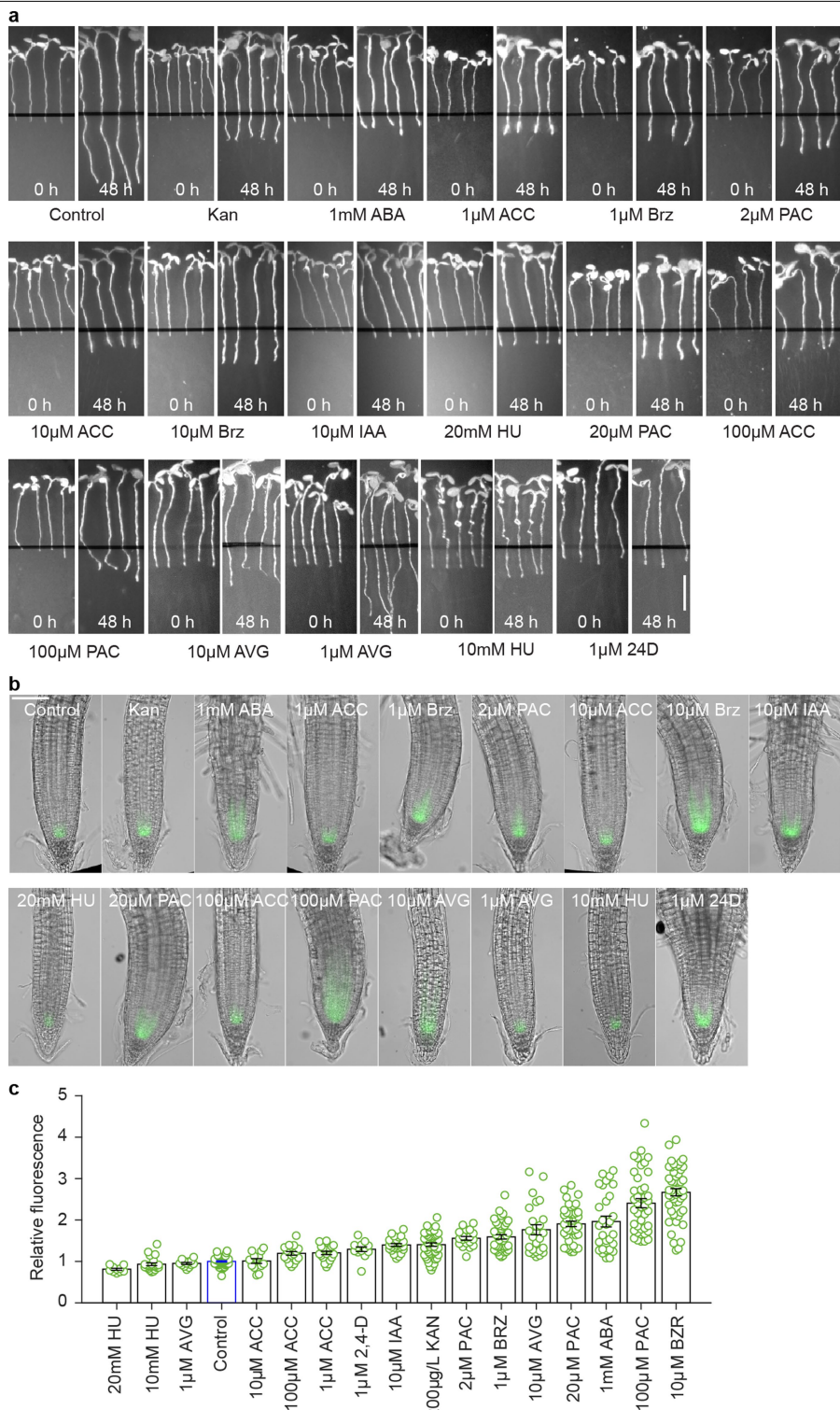


Extended Data Fig. 6 | Analysis of NTL8 isoforms in WT plants, and assay of NTL8 protein turnover rate under CHX treatment. **a**, Schematic of *NTL8* RNA isoforms identified by 3'RACE and sequence of isoforms 2 and 3. The red arrows indicate the differences of isoform 2 and isoform 3 from isoform 1. **b**, Quantification of protein concentration from western blots of Fig. 2a and additional replicates of experiment, showing each band separately. **c**, Quantification of the transcript levels of all three isoforms by qPCR. NV: 20 °C. 4W indicates 4 weeks of treatment in the vernalization room at 5 °C. Error bars are s.e.m. of eight (for isoform 1) or four (for isoform 2 and isoform 3) biological replicates. **d**, Comparison of the proteins produced by WT *NTL8**prom*::GFP-*NTL8* and mutant *NTL8**prom*::GFP-*NTL8-D2*. The first band produced in the GFP-*NTL8* line is absent in the GFP-*NTL8-D2* line. On the basis of the sequence of GFP-*NTL8-D2*, the full-length form with the TM domain cannot be made. This suggests that the absent band corresponds to full length GFP-*NTL8*. The second band produced in the GFP-*NTL8* line matches the size on the gel of the GFP-*NTL8-D2* form. Ponceau staining of the input on separate gels was used for the loading control. For gel source data, see Supplementary Fig. 1. Two independent repeats with similar results were performed. **e**, Diagram of the predicted proteins produced by alternative splicing. The *NTL8* isoform 2 (286 aa) has a similar amino acid number as the *NTL8-D2* (293 aa) form. Given that the second

band for GFP-*NTL8* in **d** matches the size on the gel of the *NTL8-D2* form, the second band could be, at least in part, produced by *NTL8* isoform 2. Furthermore, the alternative splicing site for isoform 3 is present in the *ntl8-D2* allele, so *NTL8* isoform 3 could still be produced by the *ntl8-D2* allele, and the resulting protein probably produces the band in the *GFP-NTL8-D2* sample that matches the third band in the WT. On the basis of the protein marker, all of the bands gave systematically larger molecular weights than those predicted by the amino acid sequence, possibly due to large post-translational modifications, potential measurement inaccuracy or a combination of the two. **f,g**, GFP-*NTL8* protein concentration determined by western blot assay. Eight-day-old seedlings were treated with 100 μM CHX in the warm (20 °C; **f**) or in the cold (5 °C; **g**), as indicated for 24 h and 48 h. Ponceau staining of the input on separate gels was used for the loading control. Quantification of band intensity is shown on each gel. Two independent repeats with similar results were performed; for gel source data, see Supplementary Fig. 1. **h,i**, Eight-day old seedlings treated with 100 μM CHX in the warm (20 °C) or the cold (5 °C), as indicated for 48 h, were imaged with the fluorescence microscope Leica DM6000 (**h**) and with the Leica SP5 confocal microscope (**i**). Root structures and dying cells are shown in **i** with propidium iodide staining. Scale bars, 100 μm. Two independent repeats with similar results were performed.

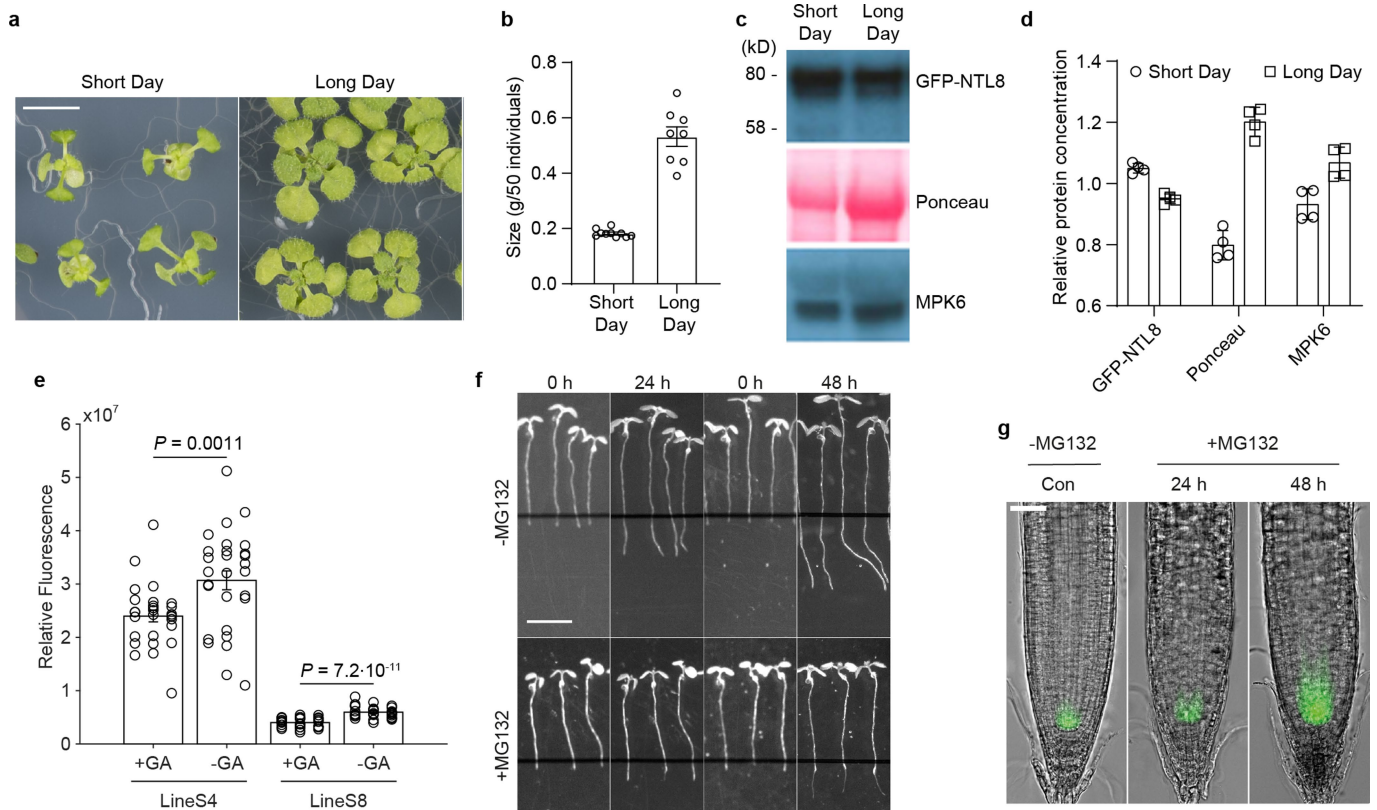


Extended Data Fig. 7 | Changes in production and growth rate are still consistent with the mathematical model. **a**, Growth rate at different temperatures estimated from the weight of 50 seedlings at different times following growth in warm (20°C) and cold (5°C) conditions. Seedlings were transferred to the cold (blue data points) after 7 days in the warm (data shown as empty circles) or 12 days (filled diamonds). Error bars are s.e.m. of six (8 days, 12 days warm) and three (all other time points) biological replicates. Linear regression was used, with the fitted lines shown together with the slopes corresponding to the growth rates in the different conditions. The difference in growth between warm and cold conditions was approximately sevenfold. The older seedlings grew faster in the cold. Therefore, we used the average slope between the growth rates of 7-day-old and 12-day-old plants in the cold as the cold growth rate. **b**, Assay of the absolute amount of NTL8 by western blot with the same number of seedlings grown for 8 days in warm (20°C) conditions and then moved to the cold (5°C) or kept in the warm (20°C), showing that the amount of NTL8 per plant increases in the warm and in the cold. Error bars are s.e.m. of 13 biological replicates. For gel source data, see Supplementary Fig. 1. We performed a one-way ANOVA test: $P=8.54 \times 10^{-10}$, $F=39.42$, $R^2=0.6865$, with the Tukey HSD post-hoc test for multiple comparisons, which showed that all three pairs (NV-Cold: $P=1.44 \times 10^{-9}$, NV-Warm: $P=0.0038$, Cold-Warm: $P=1.55 \times 10^{-5}$) are significantly different. **c**, Model from Fig. 3c (no degradation) reproduced for comparison ($\alpha=1/4$, $t_{\text{div}}(\text{cold})=7$ days). **d**, Same model with a fourfold longer division time ($\alpha=1/4$, $t_{\text{div}}(\text{cold})=28$ days), showing accumulation that saturates more slowly. **e**, Model with decreased production ($\alpha=1/8$, $t_{\text{div}}(\text{cold})=7$ days). The timescale of the accumulation does not change, but the saturated levels are decreased, thus increasing the requirement for reduced dilution to explain the experimentally observed accumulation. **f**, Model with decreased production and a fourfold longer division time ($\alpha=1/8$, $t_{\text{div}}(\text{cold})=28$ days), showing that further reduced dilution can recover some of the effect due to decreased production. **g**, Table of parameters of the model from Fig. 3a–c.


Extended Data Fig. 8 | Additional treatments to reduce growth rate.

a, Inhibition of growth by applying Kan (200 µg/l), AVG (1 µM or 10 µM), ABA (1 mM), 24D (1 µM), IAA (10 µM), Brz (1 µM or 10 µM), ACC (1 µM, 10 µM or 100 µM), HU (10 mM or 20 mM) and PAC (2 µM, 20 µM or 100 µM). Control indicates no treatment. Seedlings grown for around 6 days were transferred to new medium supplemented with the indicated chemicals for 2 days in the warm (20 °C). Two independent experiments showed similar results. Scale bar, 0.5 cm. **b**, Imaging of the fluorescence signal of GFP-NTL8 in the root tip of plants from **a** after treatments for 2 days in the warm (20 °C). Scale bar, 100 µm. **c**, Quantification of the fluorescence intensity averaged over multiple roots. Two independent experiments were combined; roots were imaged per

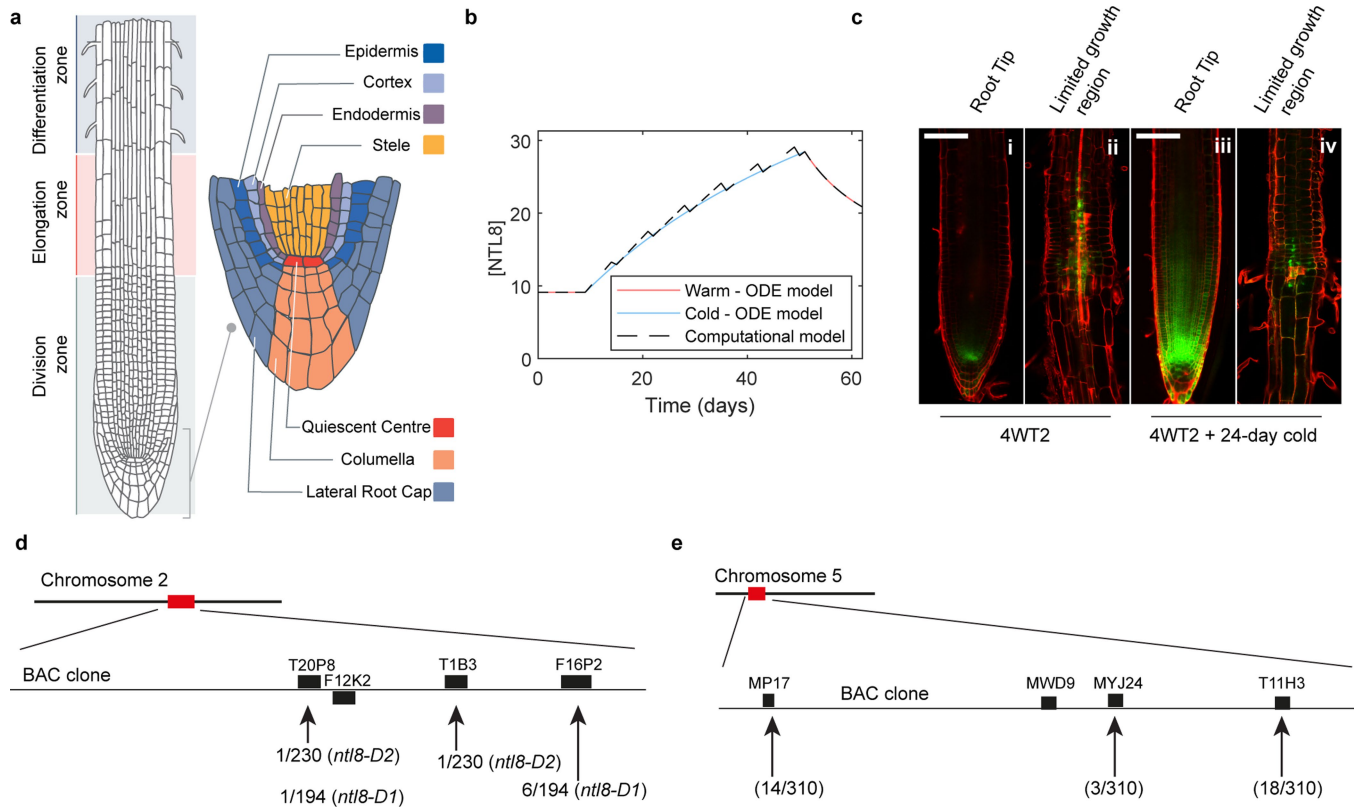
treatment (treatment order as in **c** from left to right): 16 roots total (6 excluded), 25 (1 excluded), 13 (0 excluded), 55 (3 excluded), 13 (0 excluded), 18 (0 excluded), 19 (0 excluded), 20 (7 excluded), 30 (3 excluded), 52 (0 excluded), 19 (0 excluded), 40 (0 excluded), 25 (0 excluded), 43 (0 excluded), 30 (1 excluded), 42 (0 excluded) and 51 (1 excluded). Error bars are s.e.m. We observed higher NTL8 in all treatments that inhibited growth without killing the plants. Seedlings treated with 10 mM or 20 mM HU for 2 days were almost dead. The 1 µM AVG treatment did not increase NTL8 levels, which is expected as growth was not slowed in that case. ACC treatments showed subtle effects, possibly due to indirect effects.



Extended Data Fig. 9 | Alternative treatments affecting growth show perturbed NTL8 levels. **a**, Seedling phenotypes. Six-day-old seedlings were treated under short-day (8-h light/16-h dark) or long-day (16-h light/8-h dark) conditions for 2 weeks in the warm (20 °C). Scale bar, 0.5 cm. **b**, Assay of growth in **a** by measuring fresh weight. The bulk of 50 individual seedlings were weighed. Error bars indicate s.e.m. of ten (for short day) or eight (for long day) replicates. **c**, Analysis of NTL8 protein concentration from treatments in **b** by western blot assay with equal weight of starting material. As shown by Ponceau staining, which differs between short-day and long-day treatments. Therefore, MPK6 was used as the loading control. Ponceau staining and MPK6 antibody of the input were performed on the same gel, separate to the NTL8 gel. For gel source data, see Supplementary Fig. 1. **d**, Quantification of the relative NTL8 protein concentration in **c** with ImageJ (normalized to short-day levels). Error bars show s.e.m. of four replicates. **e**, Effect of GA treatment on NTL8

accumulation in the cold. Eight-day-old seedlings grown in the warm (20 °C) were transferred to a new medium supplemented with or without GA (10 µM) and treated for 4 weeks in the cold (5 °C) before imaging. Quantification of fluorescence intensity; roots were imaged per treatment (treatment order as in **e** from left to right): 28 roots total (0 excluded), 28 (0 excluded), 31 (0 excluded) and 31 (1 excluded). Error bars are s.e.m. For comparison between treatments with and without GA, one-tailed t-test was performed: for lineS4: $t = -3.21$, d.f. = 54, $P = 0.0011$; for lineS8: $t = -7.75$, d.f. = 59, $P = 7.2 \times 10^{-11}$. **f**, Inhibition of growth by applying MG132 (100 µM). -MG132 indicates no treatment. Seedlings grown for around 6 days in the warm (20 °C) were transferred to new medium supplemented with the indicated chemicals for 2 days in the warm (20 °C). Scale bar, 0.5 cm. **g**, Imaging of the fluorescence signal of GFP-NTL8 in the root tip of plants from **f** after treatments for 24 h and 48 h. Scale bar, 50 µm. Six independent repeats with similar results were performed.

Article



Extended Data Fig. 10 | Root tissue structure and computational model of the root, NTL8 protein stability, and map-based cloning of *ntl8-D* and *ntl14-D* mutations. **a**, Diagram of root structure showing the division zone, elongation zone and differentiation zone, as well as the different tissue types in the meristematic region. Modified from ref.⁴⁰. **b**, Analytical solution of the ODE model (solid line) and the computational simulation (dashed line) of the growth dilution model give the same predicted NTL8 concentration pattern. A small difference is seen in the cold because, in the simulation, division is occurring in a single step every week, as opposed to the smooth, averaged growth of the ODE model. **c**, NTL8 protein is stable over timescales of weeks. 4-week cold (5 °C) root imaged after a further 2 days in the warm (20 °C; 4WT2; i and ii), or

24 days in the cold (5 °C) following the 2-day warm treatment (iii and iv). i and iii show the root tip, and ii and iv show the region of the root where NTL8 accumulated during the 4-week cold period. NTL8 is maintained at those high levels after transfer to warm (ii), due to limited further growth in that region, and persists there after transfer back to the cold for at least 24 days (iv). Root structures and dying cells are shown with propidium iodide staining. Scale bars, 100 μm. Two roots were imaged. **d**, Diagram of map-based cloning for *ntl8-D1* and *ntl8-D2*. Recombination numbers are indicated separately for *ntl8-D1* and *ntl8-D2* mutants. The diagram was drawn according to ref.⁴¹. **e**, Diagram of map-based cloning for *ntl14-D*. Recombination numbers are indicated as shown. The diagram was drawn according to ref.⁴².

Reporting Summary

Nature Research wishes to improve the reproducibility of the work that we publish. This form provides structure for consistency and transparency in reporting. For further information on Nature Research policies, see our [Editorial Policies](#) and the [Editorial Policy Checklist](#).

Statistics

For all statistical analyses, confirm that the following items are present in the figure legend, table legend, main text, or Methods section.

n/a Confirmed

- The exact sample size (n) for each experimental group/condition, given as a discrete number and unit of measurement
- A statement on whether measurements were taken from distinct samples or whether the same sample was measured repeatedly
- The statistical test(s) used AND whether they are one- or two-sided
 - Only common tests should be described solely by name; describe more complex techniques in the Methods section.*
- A description of all covariates tested
- A description of any assumptions or corrections, such as tests of normality and adjustment for multiple comparisons
- A full description of the statistical parameters including central tendency (e.g. means) or other basic estimates (e.g. regression coefficient) AND variation (e.g. standard deviation) or associated estimates of uncertainty (e.g. confidence intervals)
- For null hypothesis testing, the test statistic (e.g. F , t , r) with confidence intervals, effect sizes, degrees of freedom and P value noted
 - Give P values as exact values whenever suitable.*
- For Bayesian analysis, information on the choice of priors and Markov chain Monte Carlo settings
- For hierarchical and complex designs, identification of the appropriate level for tests and full reporting of outcomes
- Estimates of effect sizes (e.g. Cohen's d , Pearson's r), indicating how they were calculated

Our web collection on [statistics for biologists](#) contains articles on many of the points above.

Software and code

Policy information about [availability of computer code](#)

Data collection	All QPCR results were collected with LightCycler® 480; All images with luciferase bioluminescence signal were collected with CCD camera (NightOwl); Microscope images were collected with different microscopes (Leica205FA stereo-microscopy, Leica SP5 confocal microscope, Leica DM6000 microscopy, Leica TCS SP8X confocal microscope and Zeiss Axio Imager fluorescence microscope) and specified in the manuscript. Images for root length were taken with Alphaimager. Images for X-ray film were scanned with scanner or Cannon Camera.
Data analysis	MATLAB Version: 9.5.0.944444 (R2018b), The MathWorks, Inc., Natick, Massachusetts, United States. R version 3.3.1 (2016-06-21), The R Foundation for Statistical Computing. Python 3.5.4 Anaconda 2.4.1 (64-bit) (default, Aug 14 2017, 13:41:13) [MSC v.1900 64 bit (AMD64)] on win32 Microsoft Excel, Office 365. Prism 8 for windows v8.04 Custom image analysis code described fully in methods section and available as supplementary file and at https://github.com/ReaAntKour/NTL8TemperatureGrowth/ . (Fiji Is Just)Image J: ImageJ 1.52i, Wayne Rasband, National Institutes of Health, USA, http://imagej.nih.gov/ij , Java 1.8.0_66(64-bit)

For manuscripts utilizing custom algorithms or software that are central to the research but not yet described in published literature, software must be made available to editors and reviewers. We strongly encourage code deposition in a community repository (e.g. GitHub). See the Nature Research [guidelines for submitting code & software](#) for further information.

Data

Policy information about [availability of data](#)

All manuscripts must include a [data availability statement](#). This statement should provide the following information, where applicable:

- Accession codes, unique identifiers, or web links for publicly available datasets
- A list of figures that have associated raw data
- A description of any restrictions on data availability

Quantitative source data for figures and full scanned images of western blots are provided with the paper. Raw images that support the findings of this study are available at doi: 10.6084/m9.figshare.12283970. Code is available as a supplementary file and at <https://github.com/ReaAntKour/NTL8TemperatureGrowth/>

Field-specific reporting

Please select the one below that is the best fit for your research. If you are not sure, read the appropriate sections before making your selection.

Life sciences Behavioural & social sciences Ecological, evolutionary & environmental sciences

For a reference copy of the document with all sections, see nature.com/documents/nr-reporting-summary-flat.pdf

Life sciences study design

All studies must disclose on these points even when the disclosure is negative.

Sample size	No statistical approach was used to predetermine sample size. Sample sizes were determined based on previous publications on similar experiments. The determined sample size was adequate as the differences between experimental groups was significant and reproducible.
Data exclusions	Following the automatic image analysis pipeline, the processed images were manually curated to exclude failed results. The exclusion criterion was based on this processing, and images where the signal appeared in the wrong part or was missed by the algorithm were excluded from further analysis. A total of 23 images out of 629 were excluded using this process. No other data exclusion was performed.
Replication	All key experimental findings were reproduced in several independent biological repeats with multiple technical replicates. The number of repeats is indicated in the figure legends. Main Conclusions were confirmed in different assays (genetic assays including forward genetics with multiple allelic mutations and confirmation by transgenics, Immunoblot assay with transgenics carrying two different tags, bioimaging with different microscopies, and computational simulation).
Randomization	Multiple, randomly selected plants from a plate were collected for each replicate. Given the small nature of the experiments, different treatments were carried out in parallel, with minimum covarying factors, and therefore further randomisation of plates was not performed
Blinding	Blinding was not necessary for the molecular biology techniques, where bias could not be introduced as samples were treated together and identically. For imaging, the same settings were used for all comparisons and the results were consistent with the automatically analysed data.

Reporting for specific materials, systems and methods

We require information from authors about some types of materials, experimental systems and methods used in many studies. Here, indicate whether each material, system or method listed is relevant to your study. If you are not sure if a list item applies to your research, read the appropriate section before selecting a response.

Materials & experimental systems

n/a	Involved in the study
<input type="checkbox"/>	<input checked="" type="checkbox"/> Antibodies
<input checked="" type="checkbox"/>	<input type="checkbox"/> Eukaryotic cell lines
<input checked="" type="checkbox"/>	<input type="checkbox"/> Palaeontology and archaeology
<input checked="" type="checkbox"/>	<input type="checkbox"/> Animals and other organisms
<input checked="" type="checkbox"/>	<input type="checkbox"/> Human research participants
<input checked="" type="checkbox"/>	<input type="checkbox"/> Clinical data
<input checked="" type="checkbox"/>	<input type="checkbox"/> Dual use research of concern

Methods

n/a	Involved in the study
<input checked="" type="checkbox"/>	<input type="checkbox"/> ChIP-seq
<input checked="" type="checkbox"/>	<input type="checkbox"/> Flow cytometry
<input checked="" type="checkbox"/>	<input type="checkbox"/> MRI-based neuroimaging

Antibodies

Antibodies used

anti-HA-peroxidase, Roche, catalog number 12013819001, clone number HA (3F10), dilution 1:4000
 anti-GFP, Roche, catalog number 11814460001, mixed clone of 7.1 and 13.1, LOT19958500, dilution 1:4000
 anti-HA-TAG, cell signaling technology, catalog number 3724s, clone number c29f4, lot: 8 and 9, dilution 1:5000
 ECLTM anti-mouse IgG, horseradish peroxidase linked whole antibody (from sheep) GPR, 1ml, GE healthcare UK limited, catalog number NXA931V, lot 14263051, dilution 1:40000

ECL TM anti-rabbit IgG, horseradish peroxidase linked whole antibody (from donkey), 1ml, GE healthcare UK limited, catalog number NA934V, lot 16953209, dilution 1:40000
anti-MPK6, Sigma-Aldrich, catalog number A7104, dilution 1:6000

Validation

All antibodies are commercial. Validation statements and relevant citation of primary antibody are available from the manufacturers:
anti-HA-peroxidase, Roche, catalog number 12013819001, clone number HA (3F10): <https://www.sigmaaldrich.com/catalog/product/roche/12013819001?lang=en®ion=GB>;
anti-GFP, Roche, catalog number 11814460001: <https://www.sigmaaldrich.com/catalog/product/roche/11814460001?lang=en®ion=GB>; also validated in Fig.2a in the manuscript, where the negative control Col-0 shows no band.
anti-HA-TAG, cell signaling technology, catalog number 3724s, clone number c29f4: <https://www.cellsignal.com/products/primary-antibodies/ha-tag-c29f4-rabbit-mab/3724>; also validated in the western shown in Fig.2d&e (lane excluded from main figure, shown in source data) with Col-0 negative control.
anti-MPK6, Sigma-Aldrich, catalog number A7104: <https://www.sigmaaldrich.com/catalog/product/sigma/a7104?lang=en®ion=GB>